COGNITIVE NEUROSCIENCE

Extended amygdala-parabrachial circuits alter threat assessment and regulate feeding

Andrew T. Luskin[1,2,3,4,5,6]*, Dionnet L. Bhatti[1,2]*†, Bernard Mulvey[3,7], Christian E. Pedersen[1,2,4,5,8,9], Kasey S. Girven[4,5,10], Hannah Oden-Brunson[1,2], Kate Kimbell[1,2], Taylor Blackburn[4], Abbie Sawyer[4], Robert W. Gereau IV[1,2,7], Joseph D. Dougherty[7,8], Michael R. Bruchas[1,2,3,4,5,6,7,9,10]‡

An animal's evolutionary success depends on the ability to seek and consume foods while avoiding environmental threats. However, how evolutionarily conserved threat detection circuits modulate feeding is unknown. In mammals, feeding and threat assessment are strongly influenced by the parabrachial nucleus (PBN), a structure that responds to threats and inhibits feeding. Here, we report that the PBN receives dense inputs from two discrete neuronal populations in the bed nucleus of the stria terminalis (BNST), an extended amygdala structure that encodes affective information. Using a series of complementary approaches, we identify opposing BNST-PBN circuits that modulate neuropeptide-expressing PBN neurons to control feeding and affective states. These previously unrecognized neural circuits thus serve as potential nodes of neural circuitry critical for the integration of threat information with the intrinsic drive to feed.

INTRODUCTION

All animals must successfully seek and consume food while avoiding environmental threats to survive. The internal state of an animal directly affects the expression of risky behaviors, such as exploring a dangerous environment to obtain rewards and maintain homeostasis. Animals must adaptively prioritize certain behaviors to appropriately respond to their internal state (*1*, *2*). While many studies have explored the interaction of metabolic need states with behavior, how mammals integrate affective-threat assessment with internal need states remains largely unknown.

Several recent reports have found that, in mammals, food consumption and threat assessment are heavily influenced by the parabrachial nucleus (PBN), a pontine structure that integrates visceral and sensory information to encode metabolic needs (*3*–*12*). The amygdala and extended amygdala are evolutionarily conserved brain regions that encode and integrate valence, stress, and threat to alter behavioral states. Anatomical data suggest that the PBN receives input from several regions that may encode affective information, including the bed nucleus of the stria terminalis (BNST), a structure in the extended amygdala (*8*, *13*–*15*). However, the neural circuit mechanisms that underlie the integration of an animal's own motivation to eat with internal affective states regarding environmental threats are still relatively unknown. Here, we identified two previously unknown afferents from distinct populations within the BNST to the PBN that integrate threat assessment and feeding signals to modulate PBN activity and ultimately regulate state-dependent feeding.

[1]Department of Anesthesiology, Washington University School of Medicine, St. Louis, MO 63110, USA. [2]Washington University Pain Center, Washington University School of Medicine, St. Louis, MO 63110, USA. [3]Division of Biology and Biomedical Sciences, Washington University School of Medicine, St. Louis, MO 63110, USA. [4]Department of Anesthesiology and Pain Medicine, University of Washington, Seattle, WA 98195, USA. [5]Center for Neurobiology of Addiction, Pain, and Emotion, University of Washington, Seattle, WA 98195, USA. [6]Graduate Program in Neuroscience, University of Washington, Seattle, WA 98195, USA. [7]Department of Genetics, Washington University School of Medicine, St. Louis, MO 63110, USA. [8]Department of Biomedical Engineering, Washington University, St. Louis, MO 63130, USA. [9]Department of Bioengineering, University of Washington, Seattle, WA 98105, USA. [10]Department of Pharmacology, University of Washington, Seattle, WA 98195, USA.
*These authors contributed equally to this work.
†Present address: Program in Neuroscience, Harvard Medical School, Boston, MA 02115, USA.
‡Corresponding author. Email: mbruchas@uw.edu

RESULTS

Anatomical and molecular characterization of opposing BNST-PBN circuits

The BNST is a heterogeneous population composed of glutamatergic, γ-aminobutyric acid (GABA)–releasing (GABAergic), and peptidergic neurons (*16*–*21*). To determine whether distinct neuronal circuits from the BNST innervate the PBN to alter feeding behaviors, we injected Cre-inducible (DIO) anterograde adeno-associated viruses (AAVs) expressing channelrhodopsin-2 (ChR2) with an enhanced yellow fluorescent protein (eYFP) reporter (AAV5-DIO-ChR2-eYFP) into the BNST of vesicular GABA transporter (vGAT)–Cre and vesicular glutamate transporter (vGLUT2)–Cre mice, which revealed robust axonal projections to the PBN from GABAergic (Fig. 1A and fig. S1, F to K) and glutamatergic (Fig. 1D) BNST neurons. To further substantiate our anterograde tracing findings, we injected retrograde AAVs (AAV2retro) expressing a Cre-inducible eYFP reporter (AAV2retro-DIO-eYFP) (*22*) into the PBN of vGAT-Cre or vGLUT2-Cre mice (fig. S1A). Retrograde tracing revealed populations of both GABAergic and glutamatergic BNST neurons that innervate the PBN (fig. S1A).

We next assessed whether these distinct populations make functional monosynaptic connections to PBN neurons using ex vivo patch-clamp electrophysiology. We collected acute brain slices containing the PBN from either vGAT-Cre or vGLUT2-Cre mice expressing DIO-ChR2-eYFP in BNST-PBN projections. We optogenetically evoked postsynaptic currents (eIPSC) and excitatory postsynaptic currents (eEPSC) in PBN neurons receiving BNST GABAergic (Fig. 1B) or glutamatergic (Fig. 1E) innervation, respectively, during whole-cell patch clamp recording. Photoactivation of GABAergic BNST terminals in the PBN evoked IPSCs that were pharmacologically blocked using GABA type A ($GABA_A$) antagonists (Fig. 1C), while photoactivation of glutamatergic BNST terminals in the PBN evoked EPSCs that were blocked using AMPA receptor/*N*-methyl-D-aspartate receptor (NMDAR) antagonists

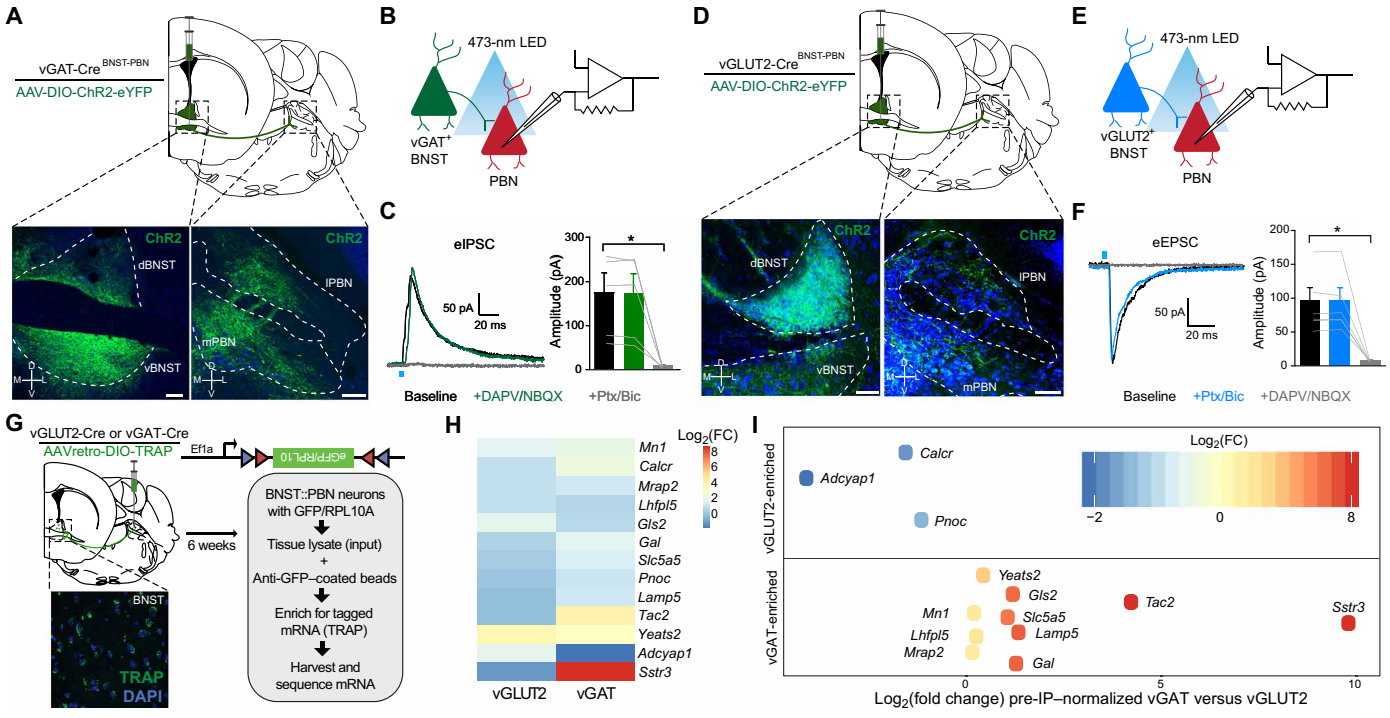

Fig. 1. Anatomical and molecular characterization of opposing BNST-PBN circuits. (**A**) Schematic of viral injection and representative image depicting expression in BNST^{vGAT} soma and their terminals in the PBN. Scale bars, 100 μm. Blue, Nissl; green, eYFP; M, medial; L, lateral; V, ventral; D, dorsal. (**B**) Schematic of whole-cell patch clamp electrophysiology recordings of optically evoked inhibitory postsynaptic currents (IPSCs). (**C**) Photoactivation of BNST^{vGAT} terminals elicits IPSCs (five of eight cells responsive) in PBN neurons that are abolished by GABA type A ($GABA_A$) receptor antagonism ($n = 5$ cells, four mice). Ptx, picrotoxin; Bic, bicuculline. (**D**) Schematic of viral injection and representative image depicting expression in BNST^{vGLUT2} soma and their terminals in the PBN. Scale bars, 100 μm. Blue, Nissl; green, eYFP. (**E**) Schematic of whole-cell patch clamp electrophysiology recordings of optically evoked excitatory postsynaptic currents (EPSCs). (**F**) Photoactivation of BNST^{vGLUT2} terminals elicits EPSCs in PBN neurons (six of nine cells responsive) that are abolished by AMPA/*N*-methyl-D-aspartate (NMDA) receptor antagonism ($n = 6$ cells, five mice). (**G**) Cartoon of injection of translating ribosome affinity purification (TRAP) into PBN of vGLUT2-Cre or vGAT-Cre animals. Tagged mRNA was extracted from the BNST and sequenced. Inset: Representative image of TRAP–green fluorescent protein (GFP) expression in BNST. (**H**) Heatmap of transcripts enriched in either vGAT or vGLUT2 projections from BNST to PBN over input homogenate [preimmunoprecipitation (pre-IP)] ($n = 3$ vGLUT2-Cre samples; $n = 2$ vGAT-Cre samples). (**I**) Transcripts enriched in either vGAT or vGLUT2 projections from BNST to PBN, after normalization to respective input (pre-IP) homogenates. Positive $\log_2$[fold change (FC)] values indicate transcript enrichment in BNST^{vGAT}-PBN neurons relative to BNST^{vGLUT2}-PBN neurons; negative $\log_2$(FC) values indicate relative enrichment in BNST^{vGLUT2}-PBN neurons. *$P < 0.05$. Error bars indicate SEM. See also figs. S1 and S2.

(Fig. 1F). Postsynaptic currents occurred <5 ms after the light pulse, suggesting that both excitatory and inhibitory connections are monosynaptic (fig. S1, B to E).

We further characterized the molecular expression profiles of these distinct inhibitory and excitatory BNST-PBN projections using translating ribosome affinity purification (TRAP) to determine their translational signature (*23*). We generated a new Cre-dependent TRAP construct within the AAV2retrovector (AAV2retro-DIO-TRAP) and injected it into the PBN of vGAT-Cre and vGLUT2-Cre mice to isolate RNA transcripts from each BNST-PBN projection population with genotype and projection specificity (*22*, *24*). We then isolated and sequenced ribosome-bound mRNA from the BNST in each group (Fig. 1G and fig. S2, A and B). The vGAT and vGLUT2 projections are enriched in several genes of interest (Fig. 1, H and I, and fig. S2, C to E). BNST^{vGAT}-PBN neurons are enriched in the neuropeptide mRNAs for tachykinin 2 (*Tac2*) (*25*) and galanin (*Gal*), as well as a somatostatin receptor (*Sstr3*) and melanocortin-2 receptor accessory protein 2 (*Mrap2*), which play important roles in regulating feeding behavior and anxiety states (*26*–*29*). BNST^{vGLUT2}-PBN neurons are enriched in *Adcyap1*, which encodes the neuropeptide pituitary adenylate cyclase-activating peptide (PACAP), previously identified as a major regulator of stress responses in the BNST (*30*, *31*), including in contexts of addiction and posttraumatic stress disorder (*32*, *33*). Both BNST^{vGAT}-PBN and BNST^{vGLUT2}-PBN neurons express calcitonin receptor (*Calcr*), recently associated with the regulation of feeding (*34*, *35*), and nociceptin (*Pnoc*), linked to motivated behaviors including feeding (*24*, *36*–*38*). We further validated these RNA sequencing (RNA-seq) findings by performing fluorescent in situ hybridization experiments, which revealed coexpression of *Tac2*, *Sstr3*, and *Calcr* with vGAT and *Adcyap1* with vGLUT2 neurons within the BNST (fig. S2, F to I).

Feeding and threat differentially engage excitatory and inhibitory BNST-PBN circuits

To determine whether these distinct genetically defined BNST-PBN circuits modulate feeding behavior, we used fiber photometry to monitor calcium-mediated fluorescence, a proxy for neuronal activity, of BNST-PBN terminals in freely behaving mice (*39*, *40*). To determine whether GABAergic BNST-PBN terminals are engaged during feeding behavior, we targeted AAVDJ-DIO-GCaMP6s to the BNST of vGAT-Cre mice and positioned optical fibers above the PBN for measurement of BNST-PBN GABAergic terminal calcium activity (Fig. 2, A and B, and fig. S3, A, C, and E). We found that BNST^{vGAT}-PBN GCaMP activity increased as an animal engaged

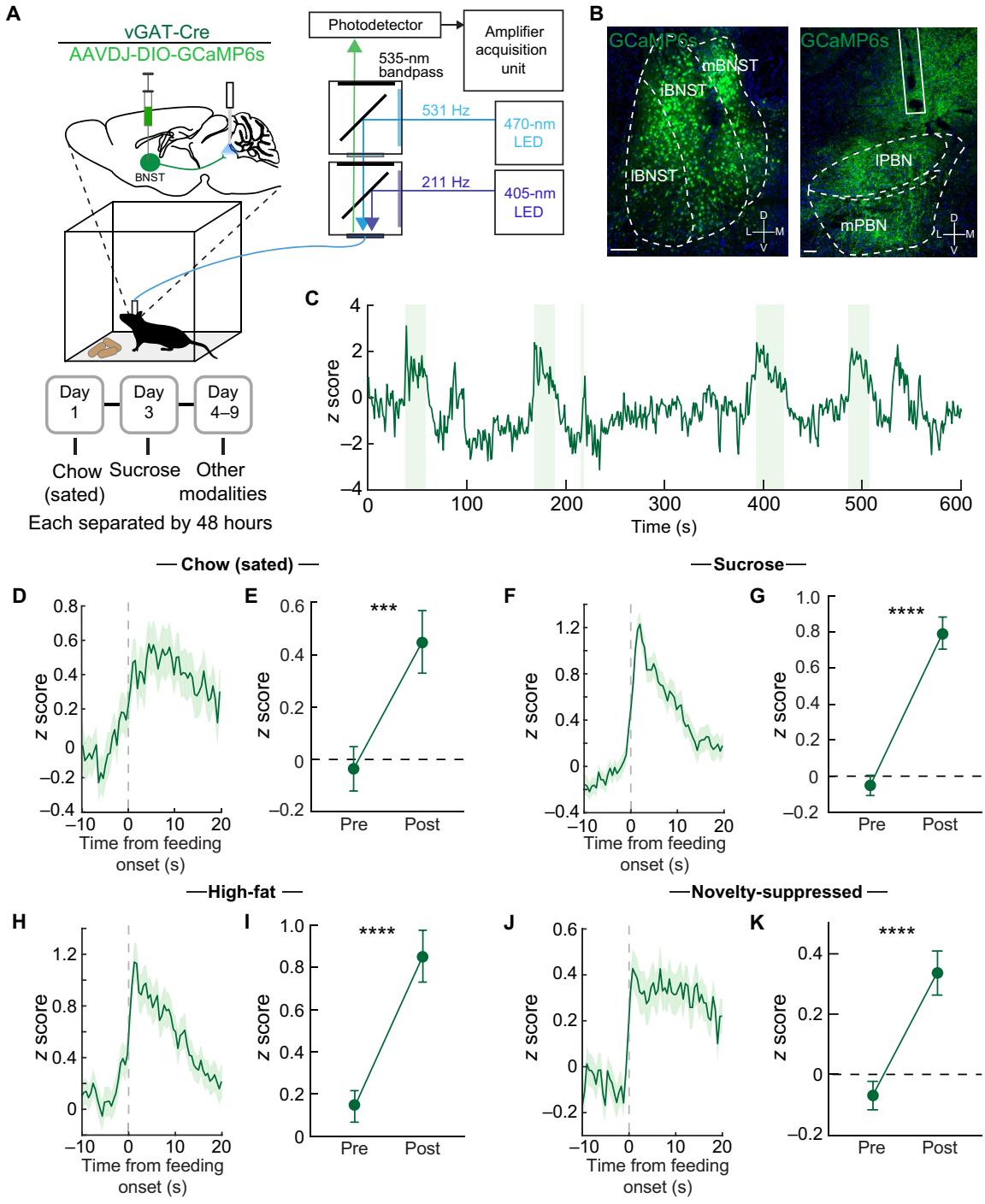

Fig. 2. Feeding behavior engages an inhibitory BNST-PBN circuit. (**A**) Schematic of in vivo fiber photometry and behavior. (**B**) Representative GCaMP6s expression in the BNST and PBN of a vGAT-Cre mouse. Scale bars, 100 μm (BNST) and 200 μm (PBN). (**C**) Representative responses of BNST^{vGAT}-PBN terminals during food consumption trials (high-sucrose chow; shaded areas represent periods of eating). (**D** and **E**) Average *z*-scored calcium response of BNST^{vGAT}-PBN terminals during consumption of normal chow under sated conditions ($n = 57$ bouts, seven mice) and averaged activity of 10-s preconsumption compared to postconsumption initiation over the testing period. (**F** and **G**) Average *z*-scored calcium response of BNST^{vGAT}-PBN terminals during consumption of sucrose ($n = 93$ bouts, seven mice) and averaged activity of 10-s preconsumption compared to postconsumption initiation over the testing period. (**H** and **I**) Average *z*-scored calcium response of BNST^{vGAT}-PBN terminals during consumption of high fat ($n = 77$ bouts, seven mice) and averaged activity of 10-s preconsumption compared to postconsumption initiation over the testing period. (**J** and **K**) Average *z*-scored calcium response of BNST^{vGAT}-PBN terminals during consumption of normal chow under anxiogenic novelty-suppressed feeding conditions ($n = 121$ bouts, seven mice) and averaged activity of 10-s preconsumption compared to postconsumption initiation over the testing period. ***$P < 0.001$, and ****$P < 0.0001$. Error bars indicate SEM. See also fig. S3.

in both sated and hedonic feeding (i.e., high-sucrose chow), as well as in other food seeking modalities including high-fat, homeostatic feeding (i.e., after food deprivation), and normal chow within novel-anxiogenic environments (Fig. 2, C to K, and fig. S3G). The increase in BNST^{vGAT}-PBN activity was greater for consumption of highly palatable high-sucrose chow and lesser in a food-deprived state, compared to consumption of normal chow under a sated condition (fig. S3I). Conversely, to assess whether glutamatergic input to the PBN is altered during feeding behavior, we targeted AAVDJ-DIO-GCaMP6s to the BNST of vGLUT2-Cre mice and similarly positioned optical fibers above the PBN for measurement of BNST-PBN glutamatergic terminal calcium activity (Fig. 3, A and B, and fig. S3, B, D, and F). In these experiments, we found that, in contrast to GABAergic BNST-PBN inputs, BNST^{vGLUT2}-PBN GCaMP activity decreased when an animal engaged in these same feeding behaviors (Fig. 3, C to K, and fig. S3H). Decreases in BNST^{vGLUT2}-PBN activity

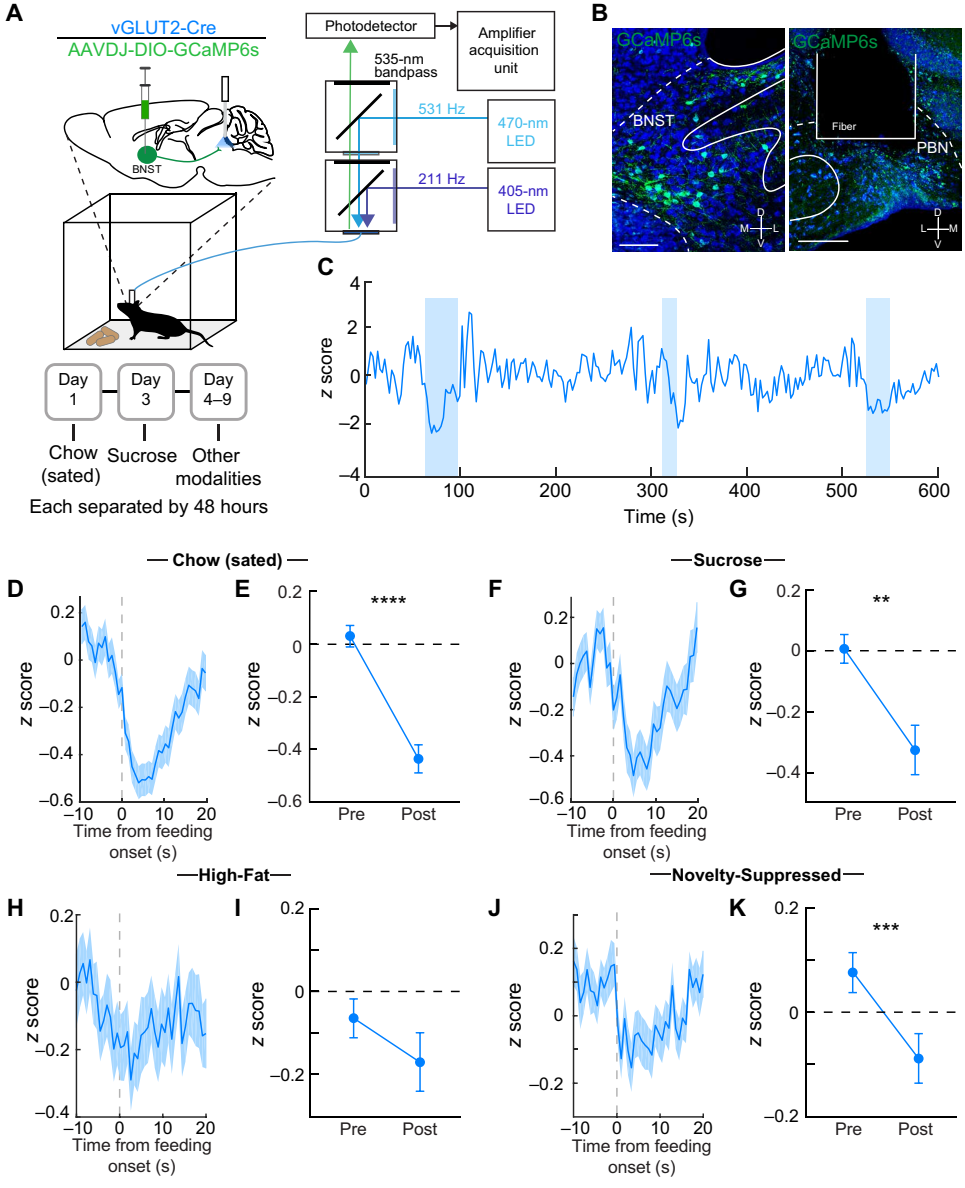

Fig. 3. An excitatory BNST-PBN circuit is disengaged during feeding. (**A**) Schematic of in vivo fiber photometry and behavior. (**B**) Representative GCaMP6s expression in the BNST and PBN of a vGLUT2-Cre mouse. Scale bars, 100 μm (BNST) and 200 μm (PBN). (**C**) Representative responses of BNST^{vGLUT2}-PBN terminals during food consumption trials (high-sucrose chow; shaded areas represent periods of eating). (**D** and **E**) Average *z*-scored calcium response of BNST^{vGLUT2}-PBN terminals during consumption of normal chow under sated conditions ($n = 133$ bouts, six mice) and averaged activity of 10-s preconsumption compared to postconsumption initiation over the testing period. (**F** and **G**) Average *z*-scored calcium response of BNST^{vGLUT2}-PBN terminals during consumption of sucrose ($n = 87$ bouts, six mice) and averaged activity of 10-s preconsumption compared to postconsumption initiation over the testing period. (**H** and **I**) Average *z*-scored calcium response of BNST^{vGLUT2}-PBN terminals during consumption of high fat ($n = 56$ bouts, six mice) and averaged activity of 10-s preconsumption compared to postconsumption initiation over the testing period. (**J** and **K**) Average *z*-scored calcium response of BNST^{vGLUT2}-PBN terminals during consumption of normal chow under anxiogenic novelty-suppressed feeding conditions ($n = 77$ bouts, six mice) and averaged activity of 10-s preconsumption compared to postconsumption initiation over the testing period. $^{**}P < 0.01$, $^{***}P < 0.001$, and $^{****}P < 0.0001$. Error bars indicate SEM. See also fig. S3.

were lesser for consumption of high-fat chow and in an anxiogenic environment, relative to normal sated chow consumption (fig. S3J). To evaluate whether these changes in activity were due simply to food presence or approach, we assessed calcium activity, while animals attempted to eat an inaccessible food item (fig. S3, U and V). Our findings demonstrate that the change in either vGAT or vGLUT2 BNST-PBN terminal activity is not associated with the approach or presence of food. When animals attempted to eat a false food item, however, we found a subtle but stable increase in BNST^{vGAT}-PBN GCaMP fluorescence (fig. S3W), consistent with the notion that this circuit is involved in food consumption. Alternatively, we observed no change in BNST^{vGLUT2}-PBN GCaMP fluorescence when animals attempted to consume false food (fig. S3X). Furthermore, neither vGAT nor vGLUT2 BNST-PBN terminals exhibited an increase in GCaMP activity when interacting with a novel or familiar object (fig. S3, Y to BB). Together, these data further support opposing roles for GABAergic and glutamatergic BNST-PBN circuits in modulating consummatory feeding behavior.

Food seeking requires an integration of threat assessment and anxiety-like behavior to adaptively seek out and consume food, as it is necessary for survival. We therefore hypothesized that if these circuits alter feeding behavior concurrently with threat assessment, then GABAergic or glutamatergic BNST-PBN input may be differentially engaged during aversive threat stimuli. To assess this, we recorded from BNST-PBN terminals in vGAT-Cre and vGLUT2-Cre mice during the presentation of multiple shock stimuli (Fig. 4A). When animals were presented with an aversive shock, BNST^{vGAT}-PBN GCaMP activity rapidly decreased in response (Fig. 4, B to D), while BNST^{vGLUT2}-PBN GCaMP activity increased following shock (Fig. 4, E to G). Similarly, BNST^{vGAT}-PBN calcium activity decreases (Fig. 4, H to J), whereas BNST^{vGLUT2}-PBN calcium activity increases (Fig. 4, K to M), upon entry into an innately anxiogenic environment such as the open arms of an elevated zero maze (EZM). Unexpectedly, no change in terminal activity in either projection arose after tone-shock associations were made and shock-predictive cues were presented alone (fig. S3, CC and DD). These observations indicate that inhibitory GABAergic BNST-PBN circuits may act to diminish threat signaling to engage and allow feeding, while excitatory glutamatergic BNST-PBN circuits are likely recruited to enhance threat signaling and suppress feeding behaviors in response to immediately threatening stimuli.

Excitatory and inhibitory BNST-PBN circuit activation induce opposing feeding behaviors

Because photometry measurements at BNST-PBN terminals revealed that these two opposing BNST-PBN projections are modulated during feeding and threat responses, we next used optogenetic approaches to assessing whether manipulating neural circuit activity of BNST-PBN circuits alters feeding, threat, and affective valence and to determine direct causality of this circuit in regulating behavior.

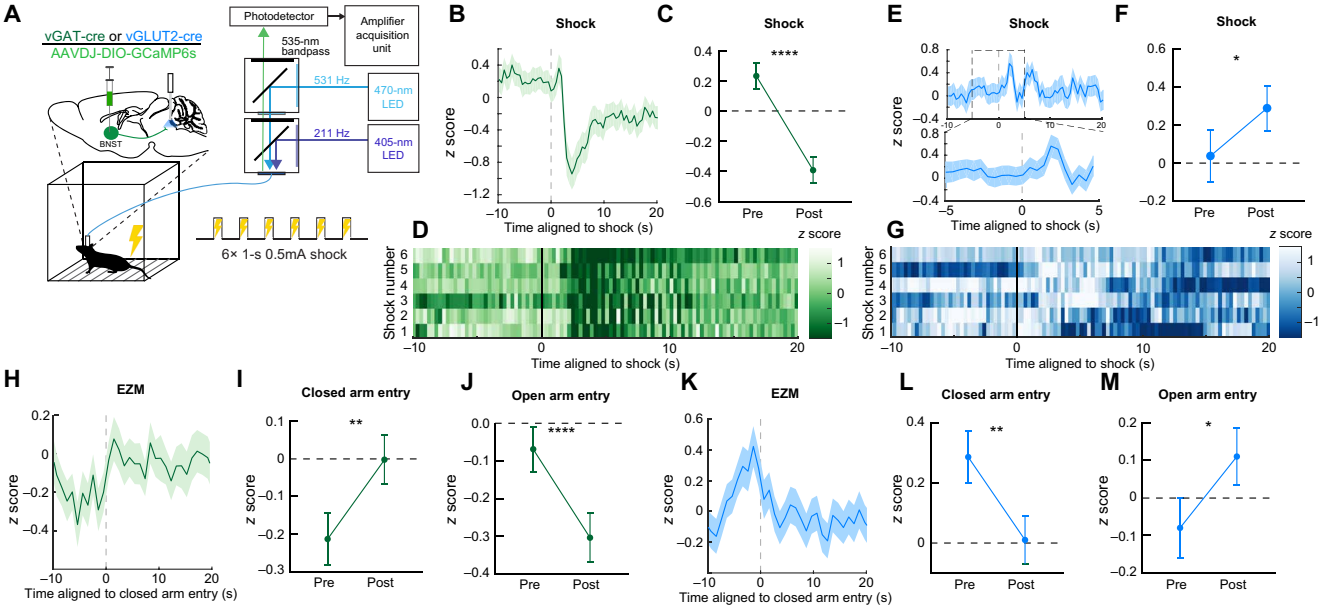

Fig. 4. Distinct BNST-PBN circuits display opposing responses to aversive stimuli. (**A**) Schematic of in vivo fiber photometry and behavior. (**B**) Average *z*-scored calcium transient responses of BNST^{vGAT}-PBN terminals to an aversive shock ($n = 7$ mice). (**C**) Mean *z*-scored calcium transient responses of BNST^{vGAT}-PBN terminals ($n = 7$ mice) 10 s before and after the shock initiation. (**D**) Representative heatmap of BNST^{vGAT}-PBN terminal calcium transient activity of a single mouse during aversive shock presentation. (**E**) Average *z*-scored calcium transient responses of BNST^{vGLUT2}-PBN terminals to an aversive shock ($n = 6$ mice). (**F**) Mean *z*-scored calcium transient responses of BNST^{vGLUT2}-PBN terminals ($n = 6$ mice) 10 s before and after the shock initiation. (**G**) Representative heatmap of BNST^{vGLUT2}-PBN terminal calcium transient activity of a single mouse during aversive shock presentation. (**H**) Average *z*-scored calcium transient responses of BNST^{vGAT}-PBN terminals to entry into the closed arm of an EZM ($n = 6$ mice). (**I**) Mean *z*-scored calcium transient responses of BNST^{vGAT}-PBN terminals ($n = 6$ mice) 5 s before and after entry into the closed arm of an EZM. (**J**) Mean *z*-scored calcium transient responses of BNST^{vGAT}-PBN terminals ($n = 6$ mice) 5 s before and after entry into the open arm of an EZM. (**K**) Average *z*-scored calcium transient responses of BNST^{vGLUT2}-PBN terminals to entry into the closed arm of an EZM ($n = 5$ mice). (**L**) Mean *z*-scored calcium transient responses of BNST^{vGLUT2}-PBN terminals ($n = 5$ mice) 5 s before and after entry into the closed arm of an EZM. (**M**) Mean *z*-scored calcium transient responses of BNST^{vGLUT2}-PBN terminals ($n = 5$ mice) 5 s before and after entry into the open arm of an EZM. *$P < 0.05$, and **$P < 0.01$. Error bars indicate SEM. See also fig. S3.

We targeted AAV5-EF1α-DIO-ChR2 to the BNST of vGAT-Cre or vGLUT2-Cre mice and positioned optical fibers above the PBN for photostimulation of BNST-PBN GABAergic or glutamatergic terminals (Fig. 5A). First, we measured food consumption with or without genetically defined neural circuit photoactivation, while mice had free access to different foods (Fig. 5B). Neurons were photostimulated at 20 Hz, consistent with previously identified firing rates in BNST projection neurons (*20*). First, to ensure that a homeostatic drive to feed was elicited by withdrawal of food, we measured food consumption under sated and food-deprived conditions (Fig. 5C). Activation of ChR2 in BNST^{vGAT}-PBN neurons increased food consumption compared to control mice under sated conditions (Fig. 5D and fig. S4A). This increase also occurred with sucrose and high-fat foods (fig. S4, C to E). No change, however, was observed when mice were in a food-deprived state (Fig. 5D and fig. S4B), suggesting that inhibitory BNST-PBN circuits are already engaged, consistent with our fiber photometry results (fig. S3G). Furthermore, photoactivation of BNST^{vGAT}-PBN signaling also increased consumption of less-palatable salt-enriched or bitter (i.e., quinine-enriched) foods (fig. S4, F to H). Moreover, BNST^{vGAT}-PBN activation is sufficient to drive animals to attempt to consume non-food items (fig. S4J). Together, these results suggest that the inhibitory BNST-PBN circuit is sufficient to drive feeding in sated states, regardless of taste modality or caloric content. In contrast to activation of BNST^{vGAT}-PBN, activation of BNST^{vGLUT2}-PBN in a food-deprived state decreased the consumption of normal chow (Fig. 5D and fig. S4, W and X), demonstrating that the excitatory BNST-PBN circuit is sufficient to reduce feeding when mice are in a food-deprived state. Photostimulation of either inhibitory or excitatory BNST-PBN circuitry did not change body temperature (fig. S4O), suggesting that the effects on feeding are independent of thermoregulation, an identified role of PBN neurons (*41*).

We next sought to determine the necessity of BNST-PBN circuits for feeding behavior. We performed projection-specific chemogenetic inhibition experiments by injecting an AAV5-DIO-hM4Di-DREADD (*42*) in the BNST of vGAT and vGLUT2-Cre mice and infusing clozapine N-oxide (CNO) into the PBN through a cannula (Fig. 5Q). We found that, in a sated state, inhibition of BNST^{vGLUT2}-PBN projections increased feeding compared to inhibition of BNST^{vGAT}-PBN projections (Fig. 5R). When animals were fasted for 24 hours, inhibition of BNST^{vGAT}-PBN projections decreased feeding relative to inhibition of BNST^{vGLUT2}-PBN neurons and control mice (Fig. 5S). These findings were also corroborated with photoinhibition of the BNST^{vGAT}-PBN circuit using Arch3.0 (fig. S4, S and T). Together, these results indicate that binary and opposing BNST-PBN circuits bidirectionally modulate food consumption.

Excitatory and inhibitory BNST-PBN circuit activation induce opposing affective states

Internal states and affective valence alter an animal's ability to assess potential threats and explore different environments, a requirement to locate and consume foods. Therefore, we assessed the affective valence of these distinct BNST-PBN circuits by subjecting mice to real-time place preference (RTPP) tests and operant-reinforcement assays (*43*–*45*). In these experiments, we injected AAV5-EF1α-DIO-ChR2 into the BNST of vGAT-Cre or vGLUT2-Cre mice, placed an optic fiber above the PBN, and tested whether stimulation of this BNST^{vGAT}-PBN pathway was appetitive or aversive. In the RTPP assay, photoactivation of ChR2 in BNST^{vGAT}-PBN neurons resulted in a robust place preference for the photostimulation-paired side, while photoactivation of ChR2 in BNST^{vGLUT2}-PBN neurons resulted in a robust place aversion for the photostimulation-paired side, as compared to controls (Fig. 5, E and F). In an operant self-stimulation paradigm (Fig. 5G), photoactivation of BNST^{vGAT}-PBN neurons significantly increased the number of nose pokes for self-stimulation relative to controls (Fig. 5H), demonstrating that BNST^{vGAT}-PBN stimulation is positively reinforcing. Conversely, photoactivation of BNST^{vGLUT2}-PBN neurons significantly increased the number of nose pokes mice performed to turn off photostimulation (Fig. 5I and fig. S4Y), demonstrating that BNST^{vGLUT2}-PBN stimulation is negatively reinforcing. These data indicate that activation of GABAergic and glutamatergic BNST-PBN circuits have innate positive and negative affective valence, respectively (*46*).

To determine whether BNST-PBN circuits modulate threat assessment, we tested mice in the EZM, which measures anxiety-like behaviors and exploration in a novel anxiogenic context (*43*). Photoactivation of BNST^{vGAT}-PBN induced an anxiolytic-like state characterized by more time spent in the open arms compared to controls (Fig. 5J and fig. S4K), consistent with increased exploratory drive. In contrast, photoactivation of BNST^{vGLUT2}-PBN neurons induced an anxiogenic-like state characterized by less time spent in the open arms (Fig. 5K), indicating that stimulation of this circuit is sufficient to reduce exploration of an anxiogenic environment. As a further test of whether BNST^{vGAT}-PBN activation can suppress defensive behaviors associated with threat, we subjected mice to threat conditioning and measured their defensive response (i.e., freezing) to a conditioned stimulus. Mice were trained to associate a conditioned stimulus (tone) with a highly aversive unconditioned stimulus (0.7 mA, 2-s foot shock). Photostimulation of BNST^{vGAT}-PBN neurons robustly reduced the defensive responses to the conditioned stimulus, likely through overriding threat responses and driving exploration associated with food seeking (Fig. 5, L and M). Photoactivation did not alter extinction retention, suggesting that BNST^{vGAT}-PBN activity may simply reduce threat responsivity. To test whether suppression of these circuits could modulate affective behaviors, we tested whether chemogenetic inhibition of BNST-PBN terminals could alter exploration in the EZM. Inhibition of BNST^{vGAT}-PBN neurons decreased exploration in an EZM (Fig. 5T). These data indicate that BNST-PBN circuits are necessary and sufficient for regulating opposing threat- and anxiety-related behavioral states.

To determine whether BNST-PBN circuitry modulates feeding in a threatening context, we performed conflict feeding assays, which pit the drive to feed against its urge to explore a novel anxiogenic environment. While stimulation of BNST^{vGLUT2}-PBN neurons decreased feeding and increased the latency to feed in under anxiogenic conditions in the open-field test (OFT), stimulation of BNST^{vGAT}-PBN neurons increased feeding (Fig. 5, N and O). Stimulation of BNST^{vGAT}-PBN neurons also increased feeding when food was placed on the open arms of the EZM (Fig. 5P and fig. S4, P and Q). Following this pattern, inhibition of BNST^{vGAT}-PBN projections decreased food consumption and increased latency to feed in an open field, while BNST^{vGLUT2}-PBN inhibition increased food consumption (Fig. 5, U and V), suggesting that this glutamatergic circuit may be selectively recruited to suppress consumption in anxiogenic or threatening environments. These results indicate that BNST-PBN circuitry can modulate feeding within anxiogenic contexts.

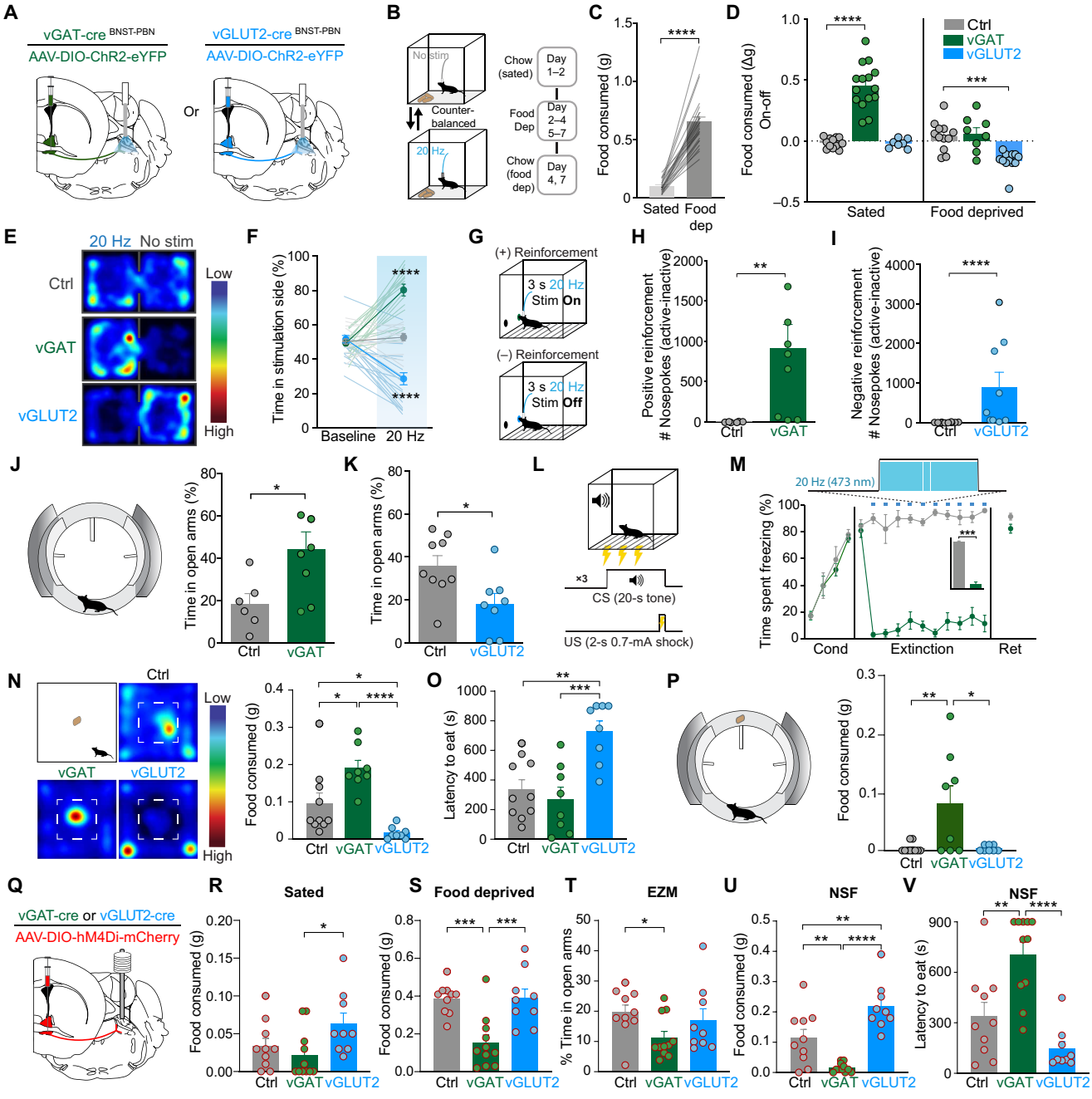

Fig. 5. Distinct BNST-PBN circuits drive opposing feeding and affective behaviors. (**A**) Schematic of optogenetic approach to targeting BNST^{vGAT}-PBN and BNST^{vGLUT2}-PBN. (**B**) Schematic of food consumption assay. (**C**) Food deprivation increases food consumption in control animals. (**D**) BNST^{vGAT}-PBN activation increases consumption of normal chow under sated conditions, whereas BNST^{vGLUT2}-PBN activation decreases consumption of normal chow after food deprivation. (**E**) Representative heatmaps of time spent in the real-time place preference (RTPP) for Ctrl, BNST^{vGAT}-PBN:ChR2, and BNST^{vGLUT2}-PBN:ChR2 mice. (**F**) BNST^{vGAT}-PBN activation elicits an RTPP, while BNST^{vGLUT2}-PBN activation elicits a real-time place aversion, compared to control mice. (**G**) Schematic of positive (BNST^{vGAT}-PBN:ChR2) and negative (BNST^{vGLUT2}-PBN:ChR2) reinforcement tasks. (**H**) BNST^{vGAT}-PBN activation is positively reinforcing in an operant-self stimulation task. (**I**) BNST^{vGLUT2}-PBN activation is negatively reinforcing in an operant task to turn off photostimulation. (**J**) BNST^{vGAT}-PBN activation increases time spent in open arms of EZM. (**K**) BNST^{vGLUT2}-PBN activation decreases time spent in open arms of EZM. (**L**) Schematic of fear conditioning protocol. CS, conditioned stimulus; US, unconditioned stimulus. (**M**) BNST^{vGAT}-PBN activation suppresses cued-defensive responses (freezing) after conditioning. (**N** and **O**) Novelty-suppressed feeding. (N) Representative heatmaps depicting exploration of the open field. BNST^{vGAT}-PBN stimulation increases food consumed and BNST^{vGLUT2}-PBN stimulation decreases food consumed. (O) BNST^{vGAT}-PBN stimulation decreases latency to feed and BNST^{vGLUT2}-PBN stimulation increases latency to feed. (**P**) Conflict feeding in EZM. BNST^{vGAT}-PBN stimulation increases food consumption. (**Q**) Schematic of chemogenetic approach to inhibiting BNST^{vGAT}-PBN and BNST^{vGLUT2}-PBN. (**R**) Inhibition of BNST^{vGLUT2}-PBN increases feeding in sated mice. (**S**) Inhibition of BNST^{vGAT}-PBN decreases feeding in food-deprived mice. (**T**) Inhibition of BNST^{vGAT}-PBN decreases exploration of EZM. (**U**) Inhibition of BNST^{vGAT}-PBN decreases food consumption and inhibition of BNST^{vGLUT2}-PBN increases food consumption in novelty-suppressed feeding assay. (**V**) Inhibition of BNST^{vGAT}-PBN increases latency to feed in novelty-suppressed feeding assay. *$P < 0.05$, **$P < 0.01$, ***$P < 0.001$, and ****$P < 0.0001$. Error bars indicate SEM. See also fig. S4 and table S1 for *n*.

Excitatory and inhibitory BNST afferents target both dynorphin and calcitonin gene-related peptide neurons in PBN

We next aimed to determine the specific targets of $BNST^{vGAT}$ and $BNST^{vGLUT2}$ projections in the PBN. Previous studies have identified diverse neuronal populations within the primarily glutamatergic PBN (*4*, *10*, *47*, *48*). The PBN contains multiple neuropeptidergic populations, including neurons that synthesize and release calcitonin gene-related peptide (CGRP) (*4*) and dynorphin (pDyn) (*47*). To further explore how PBN neurons downstream of BNST-PBN circuits regulate feeding and affective behaviors, we examined the organization of PBN dynorphin (pDyn) neurons, previously shown to regulate thermoregulation (*47*, *49*) and ingestion in response to mechanosensory feedback (*12*), and CGRP neurons (*4*–*6*), shown to function as a general alarm system that responds to threats and inhibits feeding when activated. In situ hybridization experiments demonstrated that pDyn neurons (PBN^{pDyn}) and CGRP neurons (PBN^{CGRP}) form genetically and anatomically distinct populations in the PBN (Fig. 6, A and B). We determined which of these populations received input from BNST projections by expressing ChR2 under a CAG promoter in BNST neurons and recording from parabrachial neurons labeled by crossing Calca (calcitonin related polypeptide alpha)-Cre mice with the fluorescent reporter line Ai14 or by injecting AAV-DIO-mCherry into the PBN of pDyn-Cre mice (Fig. 6C). We performed ChR2-assisted circuit mapping via whole-cell patch clamp recording of these genetically defined PBN neurons while photoactivating BNST terminals expressing ChR2 (*50*). Photostimulation of BNST terminals in the PBN elicited eIPSCs and eEPSCs that were abolished with bath application of tetrodotoxin (TTX) and then restored with 4-aminopyridine (4-AP) demonstrating the BNST forms monosynaptic connections with pDyn- and Calca-expressing PBN neurons (Fig. 6, D and G). We also found that photostimulation of BNST terminals evoked small EPSCs in separate pDyn and CGRP neurons that were blocked with TTX and could not be restored with application of 4-AP, indicating polysynaptic connections (Fig. 6, E and H). pDyn- and CGRP-expressing PBN neurons receive distinct proportions of excitatory and inhibitory BNST input. About 62% of PBN^{pDyn} neurons receiving monosynaptic connections from the BNST received both eIPSCs and eEPSCs, while the remaining 38% received only eEPSCs (Fig. 6I). In contrast, about 83% of PBN^{CGRP} neurons received both eIPSCs and eEPSCs, whereas the remaining 17% received only eIPSCs (Fig. 6J). Furthermore, using transynaptic rabies tracing (*51*–*53*), we found that BNST neurons form monosynaptic connections with pDyn-expressing neurons in the PBN (fig. S5, A to C). These data reveal that both inhibitory and excitatory BNST-PBN circuits modulate the activity of both pDyn- and Calca-expressing PBN neurons. These data position both PBN^{CGRP} and PBN^{pDyn} as critical downstream nodes for the behavioral effects of inhibitory and excitatory BNST-PBN inputs. Nonetheless, how PBN^{pDyn} modulates affective-feeding behaviors has not been thoroughly investigated.

pDyn-expressing PBN neurons modulate feeding and affective behavior

To understand PBN^{pDyn} dynamics during both feeding and affective behaviors, we injected AAVDJ-DIO-GCaMP6s into the PBN of pDyn-Cre mice and used photometry through fibers implanted in the PBN to track the calcium activity of PBN^{pDyn} neurons (Fig. 7A). We found that PBN^{pDyn} cell bodies increased their activity when animals consumed chow in a safe environment (Fig. 7B), consistent with a recent report (*12*). This increase also occurs during feeding in an anxiogenic open field (Fig. 7C). Furthermore, shock elicited rapid activation of PBN^{pDyn} activity, which was followed by a decrease (Fig. 7D). PBN^{pDyn} neurons decreased activity in response to a conditioned threat-predictive cue (fig. S5, D and E) and upon entry into the open arms of EZM (Fig. 7E), suggesting that the activity of this neuronal population may increase to immediately aversive events but be suppressed when threats are unclear or less imminent. PBN^{pDyn} activity did not change when animals chewed a false food pellet, sniffed inaccessible food, or interacted with a novel or familiar object (fig. S5, F to I). Together, these data support the conclusion that PBN^{pDyn} neurons are engaged during feeding and disengaged when exploring anxiogenic environments.

To further assess whether PBN^{pDyn} activation is sufficient to alter feeding and affective behaviors, we targeted dynorphin-expressing PBN neurons in pDyn-Cre mice with AAV5-EF1α-DIO-ChR2 and subjected the mice to both feeding and affective behavioral tests (Fig. 7, F and G). Consistent with the effects of excitatory BNST-PBN activation, we found that photostimulation of PBN^{pDyn} produces a robust real-time place aversion (Fig. 7, H to J, and fig. S5K) and reduced feeding when animals were in a food-deprived state (Fig. 7K and fig. S5L). In addition, inhibition of the broader glutamatergic PBN population rapidly and reversibly increased food consumption (fig. S5, M and N). Likewise, chemogenetic inhibition of PBN^{pDyn} neurons using the hM4Di DREADD strategy (Fig. 7, L and M) (*42*) decreased the latency to consume food in an anxiogenic environment and increased overall food consumption in mice expressing the inhibitory DREADD when given CNO compared to saline, while control animals did not differ between treatments (Fig. 7, N to P). Consistent with this finding, the inhibition of PBN^{pDyn} neurons produced and anxiolytic-like state in the EZM test after CNO treatment (Fig. 7Q and fig. S5, O and P). These data reveal a complex, previously unrecognized functional role of PBN^{pDyn} neurons as important integrators of BNST afferents, likely alongside PBN^{CGRP} neurons, that contribute to coordinating feeding drive, together with peripheral threat and affective information.

DISCUSSION

These studies indicate that discrete, neuropeptide-expressing, opposing neural circuitry from the BNST to the PBN modulates affective valence, threat assessment, and feeding behavior. The BNST has been shown to be involved in numerous functions related to threats and motivated behaviors (*54*), and our findings demonstrate that the BNST conveys sensory and affective information to two key neuropeptide containing populations (pDyn and Calca) in the PBN to alter behavior critical to an animal's survival.

Recent studies have demonstrated BNST input to the PBN and revealed that BNST neurons may influence respiration and anxiety via increased metabolic activity in the PBN (*13*, *15*). However, studies to date had not determined the identity of these projections. Using the use of genetic targeting in our study, we unveil a separable role for discrete genetically defined BNST-PBN projections. We also identify the complement of mRNAs actively translated by PBN-projecting BNST neurons in a cell type–specific manner, revealing several neuropeptides and their G protein–coupled receptors (GPCRs) that may act as important neuromodulatory regulators influencing affect and feeding (Fig. 1, G to I). Notably, these neuropeptides and receptors provide an entryway to follow up studies and aid the development of unique therapeutic strategies for

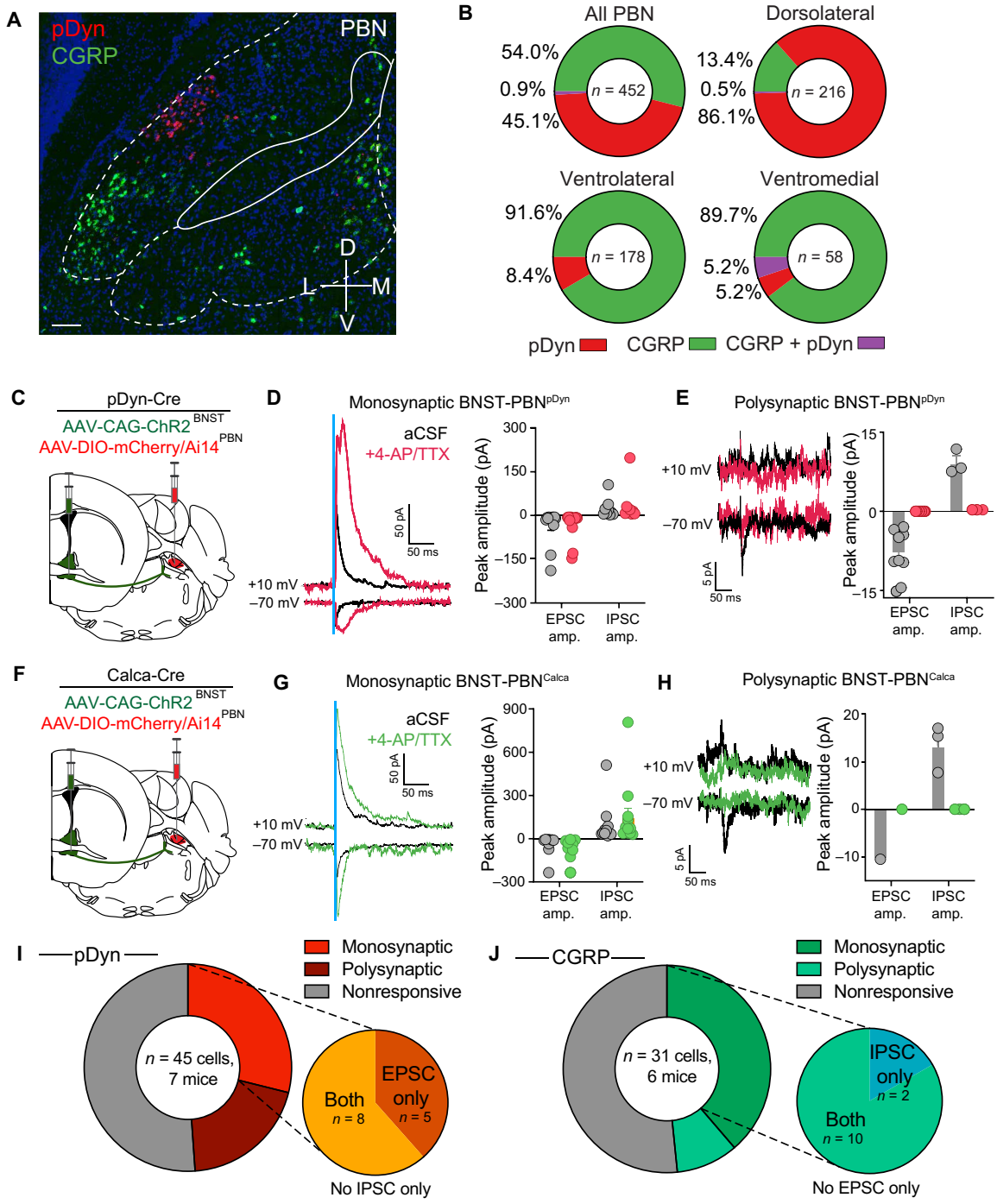

Fig. 6. Dynorphin- and CGRP-expressing PBN neurons receive both excitatory and inhibitory BNST input. (**A**) Fluorescent in situ hybridization of pDyn and CGRP in the PBN. Scale bar, 100 μm. (**B**) pDyn and CGRP neurons are genetically and anatomically distinct populations in the PBN ($n = 452$ cells). Plots represent the percentage of all labeled cells. (**C**) Schematic of virus injection depicting CAG-ChR2 in the BNST and DIO-mCherry in the PBN of pDyn-Cre mice. (**D**) Photoactivation of BNST terminals evoked monosynaptic IPSCs (top trace, +10 mV) and EPSCs (bottom trace, −70 mV) in PBN-Dyn neurons that were restored with bath application of 4-aminopyridine (4-AP) and tetrodotoxin (TTX) (purple trace; $n = 13$ cells, seven mice). (**E**) Photoactivation of BNST terminals evoked polysynaptic IPSCs (top trace, +10 mV) and EPSCs (bottom trace, −70 mV) in PBN-Dyn neurons that were blocked with bath application of TTX and could not restored with 4-AP ($n = 9$ cells, seven mice). (**F**) Schematic of virus injection depicting CAG-ChR2 in the BNST and DIO-mCherry in the PBN of Calca-Cre mice. (**G**) Photoactivation of BNST terminals evoked monosynaptic IPSCs (top trace, +10 mV) and EPSCs (bottom trace, −70 mV) in PBN-Calca neurons that were restored with bath application of 4-AP and TTX (purple trace; $n = 12$ cells, six mice). (**H**) Photoactivation of BNST terminals evoked polysynaptic IPSCs (top trace, +10 mV) and EPSCs (bottom trac, −70 mV) in PBN-Calca neurons that were blocked with bath application of TTX and could not restored with 4-AP ($n = 3$ cells, six mice). (**I**) Pie charts depicting the proportion of PBN-Dyn neurons receiving monosynaptic, polysynaptic, or no input from the BNST, as well as the proportion of the evoked monosynaptic currents that are inhibitory or excitatory. (**J**) Pie charts depicting the proportion of PBN-Calca neurons receiving monosynaptic, polysynaptic, or no input from the BNST, as well as the proportion of the evoked monosynaptic currents that are inhibitory or excitatory.

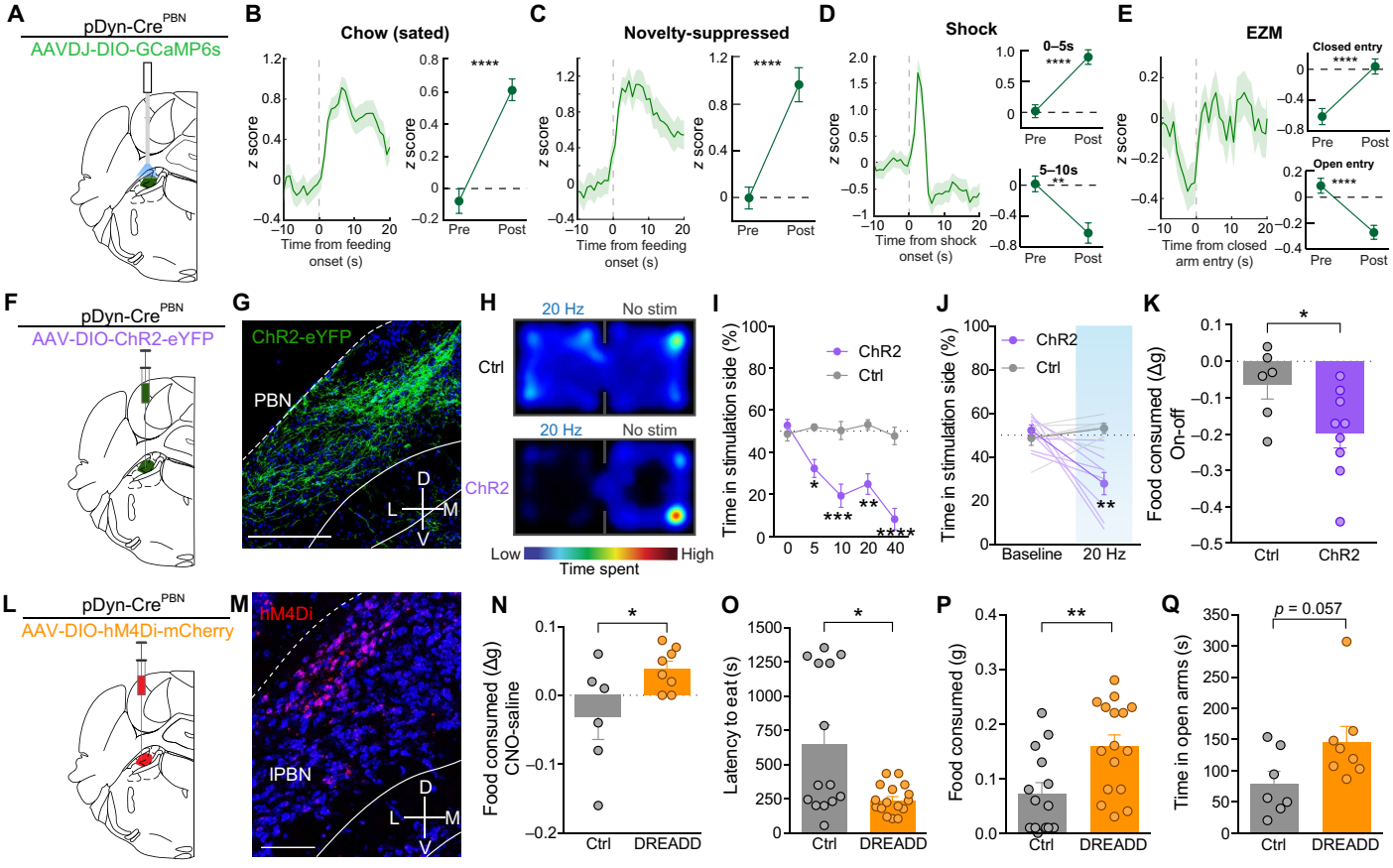

Fig. 7. Dynorphin-expressing PBN neurons mediate feeding and affective behavior. (**A**) Schematic of in vivo fiber photometry. (**B**) Average *z*-scored calcium response of PBN^{pDyn} terminals during consumption of normal chow under sated conditions ($n = 68$ bouts, six mice) and averaged activity of 10-s preconsumption versus postconsumption initiation. (**C**) Average *z*-scored calcium response of PBN^{pDyn} terminals during consumption of normal chow under anxiogenic conditions ($n = 39$ bouts, six mice) and averaged activity of 10-s preconsumption versus postconsumption initiation. (**D**) Average *z*-scored calcium response of PBN^{pDyn} terminals to an aversive shock ($n = 25$ bouts, six mice) and averaged activity of 5 s before shock initiation compared to 5 s after (top) and 5 to 10 s after (bottom) shock initiation. (**E**) Average *z*-scored calcium response of PBN^{pDyn} terminals to entry into the closed arm of an EZM and averaged activity of 5 s before and after entry into the closed arm (top; $n = 75$ bouts, six mice) and open arm (bottom; $n = 75$ bouts, six mice). (**F**) Schematic of optogenetic approach to targeting PBN^{pDyn} neurons. (**G**) ChR2-eYFP expression in PBN^{pDyn} neurons. Scale bar, 200 μm. (**H**) Representative heatmaps of time spent in RTPP for Ctrl and PBN^{pDyn}:ChR2 mice. (**I** and **J**) PBN^{pDyn} activation elicits a real-time place aversion in a (I) frequency-dependent manner, including (J) 20 Hz (ChR2, $n = 8$; Ctrl, $n = 6$). (**K**) PBN^{pDyn} activation decreases food consumption after food deprivation (ChR2, $n = 8$; Ctrl, $n = 6$). (**L**) Schematic of chemogenetic approach to targeting PBN^{pDyn} neurons. (**M**) hM4Di-mCherry expression in PBN^{pDyn} neurons. Scale bar, 100 μm. (**N** to **Q**) Chemogenetic inhibition of PBN^{pDyn} neuron (N) increases food consumption and (O) decreases latency to eat while (P) increasing food consumed in a novelty-suppressed feeding task and (Q) increasing time spent in the open arms of EZM (DREADD, $n = 7$ to 8; Ctrl, $n = 6$ to 7). *$P < 0.05$, **$P < 0.01$, ***$P < 0.001$, and ****$P < 0.0001$. Error bars indicate SEM. See also fig. S5.

treating feeding and affective diseases. Future studies using Cre driver lines and selective pharmacological approaches will be critical to dissect the neuropeptide and GPCR systems influencing these complex anxiety-like and feeding behaviors.

In this study, we also probe the neural dynamics and functional roles of opposing BNST-PBN circuits using fiber photometry together with optogenetics. Our results reveal that the GABAergic BNST-PBN circuit is engaged by and drives feeding behavior and exploration, while the glutamatergic BNST-PBN circuit is disengaged during feeding and suppresses state-dependent feeding and exploration (Figs. 2 to 5). These distinct circuits are engaged differentially depending on the internal state of the animal, as well as the palatability of the food being consumed (fig. S3, I to J). While hedonic feeding (i.e., sucrose consumption) engaged the BNST^{vGAT}-PBN circuit greater than that of sated chow, homeostatic feeding (i.e., food-deprived) resulted in smaller changes relative to that of sated chow (fig. S3I). It is possible that in a food-deprived state, BNST^{vGAT}-PBN circuits are already engaged and, thus, dynamic range from fiber photometry recordings dilutes the signal change in response to feeding. This is consistent with the ceiling effect on feeding observed in BNST^{vGAT}-PBN activation in a food-deprived state (Fig. 5D and fig. S4B). In contrast, the magnitude of BNST^{vGLUT2}-PBN terminal activity to high-fat consumption is decreased compared to that of chow in a sated state (fig. S3J). These results could also suggest that the degree by which BNST^{vGLUT2}-PBN activity is decreased depends on the palatability of the food.

It is notable that BNST^{vGAT}-PBN activation elicits consummatory behavior even in the absence of hedonic drive, metabolic need, or caloric content (fig. S4, F to J). However, the consummatory response to circuit activation is affected by food deprivation (fig. S4, A, B, V, and W), and the fiber photometry data presented here (fig. S3, I to J, W, and X) suggest that the endogenous activity of this

circuit is sensitive to internal state and food palatability. We also observed that artificial, selective BNST^{vGAT}-PBN recruitment produces indiscriminate feeding behavior for feeding initiation, but not continuous consumption itself, such that photoactivation during palatable food consumption results in continuous feeding, whereas bitter or false-food items result in intermittent feeding. This effect is reflected by the lower photoactivation-induced consumption for those items (fig. S4, F to H and J). These results further support the conclusion that BNST-PBN circuitry is not solely recruited during generalized motor responses associated with consumption but is directly responsive to food palatability and internal metabolic need state.

In addition, when food consumption occurs in an anxiogenic environment (i.e., *N*-ethylmaleimide–sensitive factor), the degree by which BNST^{vGLUT2}-PBN decreases is attenuated compared to sated and safe chow consumption. This change in magnitude may reflect the increased exploratory drive necessary to overcome the animal's aversion to the center of the open field, which occurs concurrently with increases in BNST^{vGLUT2}-PBN activity when the animal explores the open zones of the EZM (Fig. 4, K to M). A highly aversive and threatening shock stimulus induced a rapid but not instantaneous (1 to 3 s) decrease or increase in activity of GABAergic and glutamatergic BNST-PBN circuits, respectively (Fig. 4, B to F), matching the peak kinetics for GCaMP6s activity in neurons with sustained firing (*55*). While acute threats may rapidly modulate neural activity, the persistence and delay in BNST-PBN circuit response to shock may represent an internal state shift resulting from the aversive experience, thus positioning these circuits as key integrators of both experience and behavior. This interpretation requires continued investigation using alternative paradigms and behavioral state changes in each case. Nevertheless, our data demonstrate that these opposing inhibitory and excitatory circuits act to drive feeding behaviors likely in part via the attribution of threat assessment and the valence inherent to the circuit itself (Fig. 5). Further studies exploring both acute and learned threat detection with opposing feeding states will be needed to explore how these circuits adapt under various environmental influences. Here, we demonstrate that selective inhibition or activation of these circuits is both necessary and sufficient to alter feeding, exploration, and threat assessment. Given that eating disorders are highly associated with varying affective states (*56*), further investigation of these circuits under varying internal states that drive motivated behaviors such as food deprivation and affective states imposed by external adverse experiences such as pain or stress is necessary to fully understand the extent of their involvement.

The PBN consists of many cell types that mediate separable aspects of feeding and aversion (*3*, *10*, *57*, *58*). Of these cell types, neurons expressing CGRP located in the ventral/external lateral parabrachial (PBNel) thought to function as a general alarm system that sends aversive signals throughout the brain are of the most notable (*59*). However, our results demonstrate that GABAergic and glutamatergic BNST terminals are most dense in the dorsolateral and medial regions of the PBN as compared to the ventrolateral region where CGRP neurons subside (Figs. 1, A and D, and 6, A and B, and fig. S1, F to K). This was both interesting and unexpected to us because this reveals that although CGRP neurons mediate feeding and aversion, they are likely not the sole neuropeptide population in the PBN mediating these behaviors. In our studies, we have demonstrated that dynorphin-expressing neurons located in the dorsolateral PBN (PBN^{pDyn}) are also critically poised as functional integrators of feeding and affective behaviors (*60*). Historically, the primary function for PBN^{pDyn} was thought to be thermoregulation (*47*, *49*). Recent studies suggest that dorsolateral and pDyn-expressing PBN neurons also respond to mechanosensory feedback and pain signals from the body to drive aversive learning and nocifensive behaviors, potentially in part by communication with CGRP neurons (*12*, *61*, *62*). Consistent with this finding, we also found here that pDyn neurons respond to noxious stimuli and environmental threats. BNST-PBN circuits thus may tune the activity of PBN neurons, including pDyn and CGRP, to modulate threat and feeding responses. Our results, alongside previous studies, indicate that a primary role for PBN^{pDyn} is to integrate a myriad of bodily signals related to internal state, such as thermoregulatory signals and pain, with limbic system signals for threat assessment and anxiety, ultimately to allow adaptive food seeking, consumption, and avoidance.

Together, we present two opposing neural circuits from the BNST to the PBN that mediate threat assessment, exploration, and feeding behaviors in part via their connections to neuropeptide-containing populations, particularly dynorphin-expressing PBN neurons. Our results implicate these circuits and both inhibitory and excitatory BNST neurons as critical integrators, with the PBN, of adaptive feeding and affective behaviors. These findings also further our understanding of the complex relationship between eating patterns and affective state.

MATERIALS AND METHODS

Animals

Adult vGAT-IRES-Cre (*Slc32a1*$^{tm2(cre)Lowl}$/J; the Jackson Laboratory, #028862) (*63*), vGLUT2-IRES-Cre (*Slc17a6*$^{tm2(cre)Lowl)}$/J; the Jackson Laboratory, #028863), and preprodynorphin (*Pdyn*)–IRES-Cre (*Pdyn*$^{tm1.1(cre)Mjkr}$/J; the Jackson Laboratory, #027958) (*64*) mice were group-housed, given access to food and water ad libitum, and maintained on a 12:12-hour light:dark cycle (lights on at 7:00 a.m.). All animals were kept in an isolated and sound-attenuated holding facility within the laboratory and adjacent to behavior rooms 1 week before surgery, after surgery, and throughout the duration of the behavioral assays to minimize stress. Males and female mice were used in all experiments with the exception of experiments in Figs. 5 (G to M) and 7 (L to Q). All procedures were approved by the Animal Care and Use Committee of Washington University and the University of Washington and conformed to U.S. National Institutes of Health (NIH) guidelines.

Stereotaxic surgeries

After the animals were acclimated to the holding facility for at least 7 days, mice were anaesthetized in an induction chamber (2% isoflurane) and placed into a stereotaxic frame (Kopf Instruments, Model 1900) where they were maintained at 1 to 2% isoflurane. Mice were then injected using a blunt needle (Hamilton, 86200) at a rate of 100 nl/min with 300 to 400 nl in the BNST [anteroposterior (AP), +0.14; mediolateral (ML), ±0.9; dorsoventral (DV), −4.5] or PBN (AP, −5.3; ML, ±1.1; DV, −3.5); unilateral for optogenetic activation, tracing, and fiber photometry experiments; and bilateral for optogenetic or chemogenetic experiments. Needle was slowly removed from the brain 10 min after cessation of injection to allow for diffusion. For fiber photometry experiments, mice were also implanted with a 400-μm fiber optic (Doric Inc., MFC_400/430-0.48_MF2.5_FLT) in the same surgery. Mice recovered for at least 6 weeks

before behavioral testing, permitting optimal expression of the virus. For optogenetic activation and fiber photometry experiments, 5 weeks after viral injection, intracranial optic fiber implants were directed above the PBN unilaterally (AP, −5.3; ML, ±1.1; DV, −3.0). For optogenetic inhibition, fiber optics were placed bilaterally. The fiber optic implants were secured using two bone screws (CMA Microdialysis AB, 743102) and affixed with TitanBond (Horizon Dental Products) and dental cement (Lang Dental).

Viruses

AAV2retro-EF1a-DIO-hChR2-(H134R)-eYFP	Hope Center Viral Vector Core, Wash.U.
AAV5-EF1a-DIO-hChR2-(H134R)-eYFP	Hope Center Viral Vector Core, Wash.U.
AAV5-CAG-hChR2(H134R)-mCherry	Addgene
AAV5-Ef1a-DIO-mCherry	University of North Carolina (UNC) Vector Core
AAV2retro-231-TRAP-Cre-On	Hope Center Viral Vector Core, Wash.U.
AAV-DJ-EF1a-DIO-GCaMP6s	Stanford University Gene Vector and Viral Core
AAV5-EF1a-DIO-Arch3.0-eYFP	UNC Vector Core
AAV5-Ef1a-DIO-hM4D(Gi)-mCherry	UNC Vector Core
AAV5-CAG-FLEX-RG	UNC Vector Core
AAV8-EF1a-FLEX-TVA-mCherry	UNC Vector Core
EnvA-G–deleted Rabies–enhanced green fluorescent protein (eGFP)	Salk

Immunohistochemistry

Immunohistochemistry was performed as previously described (*65*). Briefly, mice were anesthetized with sodium pentobarbital and transcardially perfused with 4% paraformaldehyde (PFA), postfixed overnight in 4% PFA, and cryo-protected in 30% sucrose for at least 24 hours. Brains were then sectioned (30 μm) and placed in 0.1 M phosphate buffer (PB) until immunohistochemistry. Free-floating sections were washed in 0.1 M phosphate-buffered saline (PBS) for 3× 10-min intervals. Sections were then placed in blocking buffer (0.5% Triton X-100 and 5% natural goat serum in 0.1 M PBS) for 1 hour at room temperature. After blocking buffer, sections were incubated in NeuroTrace (1:400; 435/455 blue fluorescent Nissl stain; Invitrogen, #N21479) for 1 hour, followed by 3× 10-min 0.1 M PBS and then 3× 10-min 0.1 M PB washes. After immunostaining, sections were mounted and coverslipped with VECTASHIELD HardSet mounting medium (Vector Laboratories, catalog no. H-1400) and imaged on a Leica TCS SPE confocal microscope. Animals that did not show targeted expression were excluded.

Fluorescent in situ hybridization

Animals were anesthetized and rapidly decapitated. Brains were quickly removed and fresh frozen in dry ice, then stored at −80°C. Sections were cut at 20 μm, mounted on slides, and stored at −80°C. Sections were fixed in 4% PFA for 15 min, dehydrated in serial ethanol concentrations (50, 70, and 100%), and processed with RNAscope (Advanced Cell Diagnostics, catalog no. 320293). Sections were hybridized with the probes listed below. Sections were then counterstained with 4′,6-diamidino-2-phenylindole (DAPI) and coverslipped. Confocal images were obtained on an Olympus FV3000RS microscope. Circular regions of interest (ROIs) were drawn around each cell, and these ROIs were then used for coexpression analysis.

RNAscope probes

CGRP (*Calca*)	Advanced Cell Diagnostics	Catalog no. 420361
Pdyn	Advanced Cell Diagnostics	Catalog no. 318771
vGAT (*Slc32a1*)	Advanced Cell Diagnostics	Catalog no. 319191
vGLUT2 (*Slc17a6*)	Advanced Cell Diagnostics	Catalog no. 319171
eGFP	Advanced Cell Diagnostics	Catalog no. 400281
Adcyap1	Advanced Cell Diagnostics	Catalog no. 405911
Sstr3	Advanced Cell Diagnostics	Catalog no. 460621
Tac2	Advanced Cell Diagnostics	Catalog no. 446391
Calcr	Advanced Cell Diagnostics	Catalog no. 494071

Slice electrophysiology

Acute brain slices were prepared using a protective cutting and recovery method (*66*). Anesthetized mice infected with AAV5-EF1a-DIO-hChR2-(H134R)-eYFP were transcadially perfused with *N*-methyl-D-glucamine (NMDG)–substituted artificial cerebrospinal fluid (aCSF) containing 93 mM NMDG, 2.5 mM KCl, 1.25 mM NaH_2PO_4, 30 mM $NaHCO_3$, 20 mM Hepes, 25 mM glucose, 5 mM ascorbic acid, 2 mM thiourea, 3 mM Na-pyruvate, 12 mM *N*-acetyl-L-cysteine, 10 mM $MgSO_4$, and 0.5 mM $CaCl_2$ (pH 7.3 to pH 7.4). Two hundred–millimeter-thick Coronal sections of the PBN were cut using a Vibratome VT1000s (Leica) and transferred to an oxygenated recovery chamber containing NMDG aCSF for 5 to 10 min at 32° to 34°C before being transferred to a holding chamber filled with modified aCSF containing 92 mM NaCl, 2.5 mM KCl, 1.2 mM NaH_2PO_4, 30 mM $NaHCO_3$, 20 mM Hepes, 25 mM glucose, 2 mM $CaCl_2$, 2 mM $MgCl_2$ (pH adjusted to 7.3 to 7.4 with NaOH), and 290 to 310 osM. Whole-cell patch-clamp recordings were made using fire-polished glass pipettes with a resistance of 3 to 5 megohms filled with 120 mM K^+ gluconate, 5 mM NaCl, 2 mM $MgCl_2$, 0.1 mM $CaCl_2$, 10 mM Hepes, 1.1 mM EGTA, 4 mM Na_2–adenosine 5′-triphosphate, 0.4 mM Na_2–guanosine 5′-triphosphate, 15 mM phosphocreatine (pH adjusted to 7.3 with KOH), and 291 mosM. BNST axonal projections in the PBN were visualized through a 40× objective using infrared (IR) differential interference contrast microscopy on an Olympus BX51 microscope, and neurons with YFP^+ axons in close proximity were identified using epifluorescent illumination. Recordings were made with Patchmaster software controlling a HEKA EPC10 amplifier. Following gigaseal formation and stable whole-cell access, currents elicited by 10-ms pulse stimulation of ChR2-containing axonal terminals and isolated by blocking AMPA/KARs (kainic acid receptors) [10 μM NBQX (2,3-dioxo-6-nitro-1,2,3,4-tetrahydrobenzo[f]quinoxaline-7-sulfonamide); Abcam], NMDARs [50 μM D-APV (D-APV=D-(-)-2-amino-5-phosphonopentanoic acid); Abcam], $GABA_A$Rs (100 μM picrotoxin and 50 μM bicuculline; Abcam) through bath application of the antagonists in aCSF solution. Neurons were voltage-clamped at −70 mV for eEPSCs and 0 mV for eIPSCs. Input resistance was monitored to maintain cells with a stable series resistance (Rs) of <35 megohms, and only these neurons were included in our analysis. eIPSC and eEPSC amplitudes were averaged across five sweeps per cell.

Viral retrograde TRAP

To specifically capture transcribed RNA from GABAergic and glutamatergic neurons synapsing on the PBN, we generated an adenoviral vector encoding a floxed fusion GFP-ribosomal protein (RPL10A) and packaged it into the retrofecting AAV serotype rAAV2-retro (*22*). This design restricts expression of the GFP·RPL10A fusion to a target (Cre-expressing) cell type and further restricts expression to cells of that type synapsing onto the transduced region.

To selectively capture transcripts from those excitatory and inhibitory neurons in the BNST synapsing onto the PBN, we delivered the floxed eGFP·Rpl10a AAV2retro into the PBN of adult male mice ages 4- to 10-m expressing Cre recombinase under a glutamatergic (vGLUT2) or GABAergic (vGAT) neuron-specific promoter. At least 6 weeks were given for surgical recovery and transgene expression before mice were euthanized for brain dissection, homogenization, and GFP-targeted immunoprecipitation (IP).

To control for stress and circadian effects on BNST transcripts between replicates, we always retrieved mice to be euthanized between 10 a.m. and 12 p.m. immediately before deep anesthetization by isoflurane, followed by rapid removal of the brain. A 1-mm coronal slab of brain tissue was collected from an AP of ±0.5 mm, an ML of ±1.2 mm, a DV of −3.8 to −4.8 mm and microdissected in ice-cold PBS containing ribonuclease inhibitors (rRNAsin, Superasin), 500 μM dithiothreitol, and cycloheximide (to arrest translation in progress to keep ribosomes associated with their RNAs for later capture). Three dissected BNSTs were pooled per replicate to minimize effects of dissection and incidental injection of structures adjacent to PBN. Pooled tissue was homogenized and processed using the standard TRAP protocol as previously described (*67*). All RNA samples were quality checked for RINe (estimated RNA integrity number) on an Agilent Tapestation 4200 (Agilent Technologies, Santa Clara, CA) using the High-Sensitivity RNA Assay Kit. All sequenced samples had an RINe of >7.5 with total mass yielded per sample ranging from 2.5 to 250 ng.

RNA samples were submitted to Washington University in St Louis' Genome Technology Access Center for library preparation and mRNA sequencing. Complementary DNAs (cDNAs) were synthesized using polyadenylate (polyA) capture (Dynal mRNA DIRECT Kit, Life Technologies, Carlsbad, CA). cDNAs were synthesized by polyA-targeted priming, followed by cDNA amplification using the Clontech SMARTer Kit (Takara Bio, Mountain View, CA).

Single-read, 50-bp RNA-seq of IP fractions and total homogenate from five replicates per cell type (20 samples total) was performed on a single lane of a HiSeq 3000 (Illumina, San Diego, CA), yielding ~350 M reads, ranging from 10 to 25 M per sample. Reads were processed using a standard pipeline of read trimming with Trimmomatic (*68*), removal of ribosomal RNA reads using BowTie (*69*), and alignment to mouse genome build 38.p5 along with gene-level feature counts using STAR aligner (*70*).

Samplewise read counts were first subsetted to those reads with a normal distribution to perform downstream differential expression analysis, as recommended for analyses in EdgeR (*71*, *72*). Gene counts were then quality checked by hierarchical clustering to rule out batch effects and off-target cell enrichment. One replicate clustered separately from all other samples and was excluded. Additional quality checks included plotting relative enrichment/depletion of vGAT/vGLUT2-specific marker genes and that of off-target cell types (e.g., astrocytes and oligodendrocytes). Ultimately, three replicates for vGLUT2 neurons and two replicates for vGAT neurons were used for analysis.

Differential expression analysis was performed in EdgeR using the following model for single cell type–enriched transcripts, where group was vGLUT2 IP, vGLUT2 input, vGAT IP, or vGAT input: Expression ~0 + group.

Enrichment in cell types was then determined using EdgeR's glmQLFtest function using contrasts of vGLUT2 Enriched = (vGLUT2 IP) − (vGLUT2 Input) and likewise for vGAT. Differential expression analysis between cell types was performed using the same model as above but with a contrast of (vGLUT2-vGAT Differential Expression) = (vGLUT2 IP − vGLUT2 Input) − (vGAT IP − vGAT Input). This contrast thus regresses potential effects of dissection heterogeneity before comparing the target immunoprecipitated cell types. Raw data can be found in the National Center for Biotechnology Information (NCBI) Gene Expression Omnibus (GEO) database (GSE133484).

Behavior

Behavioral assays were performed in sound attenuated rooms maintained at 23°C. Lighting was measured and stabilized at ~100 lux for anxiety testing in vGAT-Cre activation and pDyn-Cre inhibition experiments, ~20 lux for anxiety testing in vGLUT2-Cre activation experiments, and ~ 200 lux for place testing. All behavioral apparatuses were cleaned with 70% ethanol in between animals. Movements were video-recorded and analyzed using EthoVision software or recorded with MediaRecorder.

Real-time place preference

Mice were placed into a custom-made unbiased, balanced two-compartment conditioning apparatus (52.5 cm by 25.5 cm by 25.5 cm) as previously described (*65*) and allowed to freely roam the entire apparatus for 30 min. Entry into one compartment triggered constant photostimulation (0 to 40 Hz; 5- to 10-mW light power), while the animal remained in the light-paired chamber. Entry into the other chamber ended the photostimulation. The side paired with photostimulation was counterbalanced across mice. Time spent in each chamber and total distance traveled for the entire 30 min trial were measured using EthoVision 8.5 (Noldus). Data are expressed as means ± SEM percent time spent in photostimulation-paired chamber.

Operant conditioning: Positive reinforcement

For positive reinforcement induced by vGAT-containing BNST-PBN projections, mice with optical fibers implanted above the PBN were trained in one 1-hour session to nose poke on a fixed-ratio 1 schedule for optical self-stimulation (3 s, 20 Hz, ~10 mW, 473 nm) in a mouse operant chamber (17.8 cm by 15.2 cm by 18.4 cm; Med Associates) (*20*). The following day, the mice were run again with the same conditions, and the number of nose pokes recorded in the hour session was recorded.

Operant conditioning: Negative reinforcement

For negative reinforcement induced by vGLUT2-containing BNST-PBN projections, mice with optical fibers implanted above the PBN were trained in one 1-hour session to nose poke on a fixed-ratio 1 schedule to turn off optical self-stimulation in a mouse operant chamber (17.8 cm by 15.2 cm by 18.4 cm; Med Associates). Constant photostimulation (20 Hz, ~10 mW, 473 nm) began at the start of each session. Each nose poke resulted in the cessation of the photostimulation for 3 s. The following day, the mice were run again with the same conditions. The number of nose pokes recorded in the hour session was recorded. About 50% of Cre^+ mice did not

learn the operant task and thus were excluded from the results as nonresponders (fig. S4Y). Nonresponders were classified as animals whose difference of responses between active and inactive was <5. These differences did not correlate to differences in anatomy and likely reflect a failure to learn the instrumental contingency.

Threat conditioning

Pavlovian threat conditioning was performed in Med Associates Fear Conditioning Chambers (NIR-022MD). This equipment consisted of a conductive grid floor inside a 29.53-cm in length by 23.5-cm in width by 20.96-cm in height chamber inside of a soundproof box lit by an IR light.

In vGAT-Cre experiments, mice were conditioned to four 20-s tones coterminating with 2-s 0.7-mA shocks on day 1. On day 2, mice were placed back into the chamber. Eleven tone presentations in the absence of shock were presented. During the first tone, no optostimulation occurred. During the next 10 tone presentations, 20-Hz blue light was delivered. On the third day, we assessed extinction recall by placing the mice into the chamber and presented the tone once. Freezing behavior was measured during all tone presentations. All fiber photometry animals were conditioned to six 20-s tones terminating with a 1-s 0.5-mA shock.

Feeding assays

Feeding assays were performed in a square plexiglass arena (27 cm by 27 cm). Chow, high-fat, sucrose, or salt pellets (Envigo) were placed in the corner of the arena. Mice were then introduced into the arena for 30 min. To record the amount of food consumed, food was measured before and after the assay; the bottom of the chamber was scraped after each trial to collect all crumbs resulting from chewing without consumption. Baseline feeding and feeding while photostimulation (20 Hz; 5- to 10-mW light power) or photoinhibition (constant; ~5-mW light power) were performed in a counterbalanced fashion across mice.

In addition to counterbalanced experiments across days, we also performed within-session manipulations to assess whether the effects are immediately reversible. Mice were introduced into the arena for 60 min: 20-min prestimulation, 20-min 20-Hz stimulation or constant inhibition, and 20-min poststimulation. Food weight was measured at each 20-min point (figs. S4, I and X, and S5N). For IP DREADD experiments, CNO (5 mg/kg; Enzo Life Sciences, catalog no. BML-NS105) was administered 30 min before testing. For intracranial experiments, CNO (3 μM, 100 nl) was administered immediately before testing.

Elevated zero maze

EZM testing was performed as described previously (*65*). The EZM (Harvard Apparatus) was made of gray plastic, 200 cm in circumference, and composed of four 50-cm sections (two opened and two closed). The maze was elevated 50 cm above the floor and had a path width of 4 cm with a 0.5-cm lip on each open section. Mice were connected to fiber optic cables, positioned head first into a closed arm, and allowed to roam freely for 7 min. Animals received 20 Hz (10-ms pulse width) photostimulation (5- to 10-mW light power). Open-arm time was the primary measure of anxiety-like behavior. For DREADD experiments, CNO (5 mg/kg; Enzo Life Sciences, catalog no. BML-NS105) was administered 30 min before testing. For intracranial experiments, CNO (3 μM, 100 nl) was administered immediately before testing.

Novelty-suppressed feeding

Novelty-suppressed feeding was performed as previously described (*73*). Briefly, mice were food deprived for 24 hours before testing and were habituated to the room for 30 min before testing. Mice were then placed in a brightly lit (200 to 300 lux) plexiglass open-field arena (50 cm by 50 cm) with a food pellet placed at the center.

EZM conflict feeding

EZM conflict feeding was performed in the EZM as described above. Briefly, mice were food deprived for 24 hours before testing and were habituated to the room for 30 min before testing. Mice were then placed in an EZM (100 lux) with a food pellet placed in the open arm for 7 min. For optogenetic experiments, animals received 20 Hz (10-ms pulse width) photostimulation (5- to 10-mW light power). For intracranial experiments, CNO (3 μM, 100 nl) was administered immediately before testing.

False food

False food testing was performed as previously described (*74*). Briefly, mice were food deprived for 24 hours before testing and were habituated to the room for 30 min before testing. Mice were then placed in a dimly lit (25 lux) plexiglass arena (27 cm by 27 cm) with a foam plug shaped like a piece of chow placed in the middle. Videos were scored for attempts to eat the false food.

Inaccessible food

Inaccessible food testing was performed as previously described (*75*). Mice were exposed to peanut butter (Jif Creamy, Costco, #917546) 1 week before trial to eliminate food neophobia. Mice were food-deprived for 24 hours before testing and were habituated to the room for 30 min before testing. Mice were then placed in a dimly lit (25 lux) plexiglass arena (27 cm by 27 cm) with peanut butter in a caged dish, allowing the mice to smell the food, but not access it, for 25 min. Videos were scored for distinct approaches to the food.

Novel object

Novel object testing was performed using a procedure modified from a previous study (*76*). Briefly, mice were habituated to the room for 30 min before testing. Mice were then placed in a dimly lit (25 lux) plexiglass arena (27 cm by 27 cm) with two identical objects (test tubes or petri dishes; counterbalanced) fixed at the corners. Mice were given 10 min to explore the objects, then returned to the homecage for 1 hour, and then were placed in the arena with one familiar object and one novel object. Objects were thoroughly cleaned with ethanol between trials. Videos were scored for interactions with each object.

Open-field test

OFT was performed as described previously (*65*) in a plexiglass arena (50 cm by 50 cm). Center zone was defined as the middle 50% of the arena size. Mice were connected to fiber optic cables, positioned head first into a closed arm, and allowed to roam freely for 20 min. Animals received 20-Hz (10-ms pulse width) photostimulation (5- to 10-mW light power). Center time was the primary measure of anxiety-like behavior.

Temperature change

Mice were habituated to the room for 30 min before testing and then were placed in a dimly lit (25 lux) plexiglass arena (27 cm by 27 cm). Animals were stimulated at 20 Hz (5 to 10 mW, 10-ms pulse width) for 10 min. Body temperature was measured rectally before and after stimulation with a UEi DT304 digital temperature logger and a Physitemp probe.

Fiber photometry

Fiber photometry recordings were performed as previously described (*24*). Briefly, an optic fiber was attached to the implanted fiber by a ferrule sleeve, and then GCaMP6s was stimulated by two light-emitting diodes (LEDs), a 531-Hz sinusoidal light (Thorlabs, M470F3),

band-pass filtered at 470 ± 20 nm, and a 211-Hz sinusoidal light (Thorlabs, M405FP1), band-pass filtered at 405 ± 10 nm. (Filter cube: Doric FMC4; LED driver: DC4104). The 470-nm signal evokes Ca^{2+}-dependent emission, while the 405-nm signal evokes Ca^{2+}-independent isosbestic control emission. Before recording, a 180-s period of GCaMP6s excitation with both light channels was used to remove the majority of baseline drift. Laser intensity at the optic fiber tip was adjusted to ~50 μW before each day of recording. GCaMP6s fluorescent signal was isolated by band-pass filtering (525 ± 25 nm), transduced by a femtowatt silicon photoreceiver (Newport, 2151), and recorded by a real-time processor (TDT RZ5P). The envelopes of 531- and 211-Hz signals were extracted in real time by the TDT program Synapse at a sampling rate of 1017.25 Hz.

Fiber recordings were analyzed using custom MATLAB scripts available on GitHub. Baseline drift due to slow photobleaching artifacts was corrected by fitting a double exponential curve to the raw trace, then the photometry trace was *z*-scored relative to the mean and SD of the signal. The mean *z* score during 10 s preceding and following an event was compared using paired *t* tests. Shuffled traces were generated by replacing event times with a random time between the beginning and end of the session.

Statistical analyses

All summary data are expressed as means ± SEM. Statistical significance was taken as $*P < 0.05$, $**P < 0.01$, $***P < 0.001$, and $****P < 0.0001$, as determined by the Student's *t* test (paired and unpaired): one-way analysis of variance (ANOVA) or one-way repeated-measures ANOVA, followed by Bonferroni post hoc tests as appropriate. Statistical analyses were performed in GraphPad Prism 6.0 or 8.0. All statistical information is listed in table S1.

Data and code availability

RNA-seq data from Fig. 1 have been deposited and are available from GEO (accession number: GSE133484). Custom MATLAB analysis code was created to appropriately organize, process, and combine photometry recording data with associated behavioral data. Analysis code for photometry from Figs. 2, 3, and 4 is available online at www.github.com/BruchasLab. The full behavioral dataset supporting the current study is available from the corresponding author upon request.

SUPPLEMENTARY MATERIALS

Supplementary material for this article is available at http://advances.sciencemag.org/cgi/content/full/7/9/eabd3666/DC1

REFERENCES AND NOTES

1. A. L. Alhadeff, Z. Su, E. Hernandez, M. L. Klima, S. Z. Phillips, R. A. Holland, C. Guo, A. W. Hantman, B. C. De Jonghe, J. N. Betley, A neural circuit for the suppression of pain by a competing need state. *Cell* **173**, 140–152.e15 (2018).
2. C. J. Burnett, C. Li, E. Webber, E. Tsaousidou, S. Y. Xue, J. C. Brüning, M. J. Krashes, Hunger-driven motivational state competition. *Neuron* **92**, 187–201 (2016).
3. C. A. Campos, A. J. Bowen, C. W. Roman, R. D. Palmiter, Encoding of danger by parabrachial CGRP neurons. *Nature* **555**, 617–622 (2018).
4. M. E. Carter, M. E. Soden, L. S. Zweifel, R. D. Palmiter, Genetic identification of a neural circuit that suppresses appetite. *Nature* **503**, 111–114 (2013).
5. S. Han, M. T. Soleiman, M. E. Soden, L. S. Zweifel, R. D. Palmiter, Elucidating an affective pain circuit that creates a threat memory. *Cell* **162**, 363–374 (2015).
6. C. A. Campos, A. J. Bowen, M. W. Schwartz, R. D. Palmiter, Parabrachial CGRP neurons control meal termination. *Cell Metab.* **23**, 811–820 (2016).
7. R. A. Essner, A. G. Smith, A. A. Jamnik, A. R. Ryba, Z. D. Trutner, M. E. Carter, AgRP neurons can increase food intake during conditions of appetite suppression and inhibit anorexigenic parabrachial neurons. *J. Neurosci.* **37**, 8678–8687 (2017).
8. G. Zséli, B. Vida, A. Martinez, R. M. Lechan, A. M. Khan, C. Fekete, Elucidation of the anatomy of a satiety network: Focus on connectivity of the parabrachial nucleus in the adult rat. *J. Comp. Neurol.* **524**, 2803–2827 (2016).
9. C. W. Roman, V. A. Derkach, R. D. Palmiter, Genetically and functionally defined NTS to PBN brain circuits mediating anorexia. *Nat. Commun.* **7**, 11905 (2016).
10. P. J. Ryan, S. I. Ross, C. A. Campos, V. A. Derkach, R. D. Palmiter, Oxytocin-receptor-expressing neurons in the parabrachial nucleus regulate fluid intake. *Nat. Neurosci.* **20**, 1722–1733 (2017).
11. D. Mu, J. Deng, K.-F. Liu, Z.-Y. Wu, Y.-F. Shi, W.-M. Guo, Q.-Q. Mao, X.-J. Liu, H. Li, Y.-G. Sun, A central neural circuit for itch sensation. *Science* **357**, 695–699 (2017).
12. D.-Y. Kim, G. Heo, M. Kim, H. Kim, J. A. Jin, H.-K. Kim, S. Jung, M. An, B. H. Ahn, J. H. Park, H.-E. Park, M. Lee, J. W. Lee, G. J. Schwartz, S.-Y. Kim, A neural circuit mechanism for mechanosensory feedback control of ingestion. *Nature* **580**, 376–380 (2020).
13. S.-Y. Kim, A. Adhikari, S. Y. Lee, J. H. Marshel, C. K. Kim, C. S. Mallory, M. Lo, S. Pak, J. Mattis, B. K. Lim, R. C. Malenka, M. R. Warden, R. Neve, K. M. Tye, K. Deisseroth, Diverging neural pathways assemble a behavioural state from separable features in anxiety. *Nature* **496**, 219–223 (2013).
14. A. M. Douglass, H. Kucukdereli, M. Ponserre, M. Markovic, J. Gründemann, C. Strobel, P. L. A. Morales, K.-K. Conzelmann, A. Lüthi, R. Klein, Central amygdala circuits modulate food consumption through a positive-valence mechanism. *Nat. Neurosci.* **20**, 1384–1394 (2017).
15. C. M. Mazzone, D. Pati, M. Michaelides, J. Di Berto, J. H. Fox, G. Tipton, C. Anderson, K. Duffy, J. M. McKlveen, J. A. Hardaway, S. T. Magness, W. A. Falls, S. E. Hammack, Z. A. McElligott, Y. L. Hurd, T. L. Kash, Acute engagement of G_q-mediated signaling in the bed nucleus of the stria terminalis induces anxiety-like behavior. *Mol. Psychiatry* **23**, 143–153 (2018).
16. W. J. Giardino, A. Eban-Rothschild, D. J. Christoffel, S.-B. Li, R. C. Malenka, L. de Lecea, Parallel circuits from the bed nuclei of stria terminalis to the lateral hypothalamus drive opposing emotional states. *Nat. Neurosci.* **21**, 1084–1095 (2018).
17. N. Z. Gungor, R. Yamamoto, D. Pare, Glutamatergic and gabaergic ventral BNST neurons differ in their physiological properties and responsiveness to noradrenaline. *Neuropsychopharmacology* **43**, 2126–2133 (2018).
18. N. Z. Gungor, D. Paré, Functional heterogeneity in the bed nucleus of the stria terminalis. *J. Neurosci.* **36**, 8038–8049 (2016).
19. S. E. Daniel, D. G. Rainnie, Stress modulation of opposing circuits in the bed nucleus of the stria terminalis. *Neuropsychopharmacology* **41**, 103–125 (2016).
20. J. H. Jennings, D. R. Sparta, A. M. Stamatakis, R. L. Ung, K. E. Pleil, T. L. Kash, G. D. Stuber, Distinct extended amygdala circuits for divergent motivational states. *Nature* **496**, 224–228 (2013).
21. J. H. Jennings, G. Rizzi, A. M. Stamatakis, R. L. Ung, G. D. Stuber, The inhibitory circuit architecture of the lateral hypothalamus orchestrates feeding. *Science* **341**, 1517–1521 (2013).
22. D. G. R. Tervo, B.-Y. Hwang, S. Viswanathan, T. Gaj, M. Lavzin, K. D. Ritola, S. Lindo, S. Michael, E. Kuleshova, D. Ojala, C.-C. Huang, C. R. Gerfen, J. Schiller, J. T. Dudman, A. W. Hantman, L. L. Looger, D. V. Schaffer, A. Y. Karpova, A designer AAV variant permits efficient retrograde access to projection neurons. *Neuron* **92**, 372–382 (2016).
23. J. P. Doyle, J. D. Dougherty, M. Heiman, E. F. Schmidt, T. R. Stevens, G. Ma, S. Bupp, P. Shrestha, R. D. Shah, M. L. Doughty, S. Gong, P. Greengard, N. Heintz, Application of a translational profiling approach for the comparative analysis of CNS cell types. *Cell* **135**, 749–762 (2008).
24. K. E. Parker, C. E. Pedersen, A. M. Gomez, S. M. Spangler, M. C. Walicki, S. Y. Feng, S. L. Stewart, J. M. Otis, R. Al-Hasani, J. G. McCall, K. Sakers, D. L. Bhatti, B. A. Copits, R. W. Gereau, T. Jhou, T. J. Kash, J. D. Dougherty, G. D. Stuber, M. R. Bruchas, A paranigral VTA nociceptin circuit that constrains motivation for reward. *Cell* **178**, 653–671.e19 (2019).
25. M. Zelikowsky, M. Hui, T. Karigo, A. Choe, B. Yang, M. R. Blanco, K. Beadle, V. Gradinaru, B. E. Deverman, D. J. Anderson, The neuropeptide Tac2 controls a distributed brain state induced by chronic social isolation stress. *Cell* **173**, 1265–1279.e19 (2018).
26. M. Asai, S. Ramachandrappa, M. Joachim, Y. Shen, R. Zhang, N. Nuthalapati, V. Ramanathan, D. E. Strochlic, P. Ferket, K. Linhart, C. Ho, T. V. Novoselova, S. Garg, M. Ridderstråle, C. Marcus, J. N. Hirschhorn, J. M. Keogh, S. O'Rahilly, L. F. Chan, A. J. Clark, I. S. Farooqi, J. A. Majzoub, Loss of function of the melanocortin 2 receptor accessory protein 2 is associated with mammalian obesity. *Science* **341**, 275–278 (2013).
27. G. Bruschetta, J. D. Kim, S. Diano, L. F. Chan, Overexpression of melanocortin 2 receptor accessory protein 2 (MRAP2) in adult paraventricular MC4R neurons regulates energy intake and expenditure. *Mol. Metab.* **18**, 79–87 (2018).
28. S. Ahrens, M. V. Wu, A. Furlan, G.-R. Hwang, R. Paik, H. Li, M. A. Penzo, J. Tollkuhn, B. Li, A central extended amygdala circuit that modulates anxiety. *J. Neurosci.* **38**, 5567–5583 (2018).
29. L. Elsilä, E. De Miguel, E. R. Korpi, P.2.036 - Somatostatin-expressing neurons in the bed nucleus of stria terminalis in anxiety- and addiction-related behaviours in mice. *Eur. Neuropsychopharmacol.* **28**, S49–S47 (2018).

30. C. W. Roman, K. R. Lezak, M. J. Hartsock, W. A. Falls, K. M. Braas, A. B. Howard, S. E. Hammack, V. May, PAC1 receptor antagonism in the bed nucleus of the stria terminalis (BNST) attenuates the endocrine and behavioral consequences of chronic stress. *Psychoneuroendocrinology* **47**, 151–165 (2014).
31. S. E. Hammack, J. Cheung, K. M. Rhodes, K. C. Schutz, W. A. Falls, K. M. Braas, V. May, Chronic stress increases pituitary adenylate cyclase-activating peptide (PACAP) and brain-derived neurotrophic factor (BDNF) mRNA expression in the bed nucleus of the stria terminalis (BNST): Roles for PACAP in anxiety-like behavior. *Psychoneuroendocrinology* **34**, 833–843 (2009).
32. O. W. Miles, E. A. Thrailkill, A. K. Linden, V. May, M. E. Bouton, S. E. Hammack, Pituitary adenylate cyclase-activating peptide in the bed nucleus of the stria terminalis mediates stress-induced reinstatement of cocaine seeking in rats. *Neuropsychopharmacology* **43**, 978–986 (2018).
33. K. J. Ressler, K. B. Mercer, B. Bradley, T. Jovanovic, A. Mahan, K. Kerley, S. D. Norrholm, V. Kilaru, A. K. Smith, A. J. Myers, M. Ramirez, A. Engel, S. E. Hammack, D. Toufexis, K. M. Braas, E. B. Binder, V. May, Post-traumatic stress disorder is associated with PACAP and the PAC1 receptor. *Nature* **470**, 492–497 (2011).
34. W. Pan, J. M. Adams, M. B. Allison, C. Patterson, J. N. Flak, J. Jones, G. Strohbehn, J. Trevaskis, C. J. Rhodes, D. P. Olson, M. G. Myers Jr., Essential role for hypothalamic calcitonin receptor–expressing neurons in the control of food intake by leptin. *Endocrinology* **159**, 1860–1872 (2018).
35. W. Cheng, I. Gonzalez, W. Pan, A. H. Tsang, J. Adams, E. Ndoka, D. Gordian, B. Khoury, K. Roelofs, S. S. Evers, A. M. Kinnon, S. Wu, H. Frikke-Schmidt, J. N. Flak, J. L. Trevaskis, C. J. Rhodes, S.-I. Fukada, R. J. Seeley, D. A. Sandoval, D. P. Olson, C. Blouet, M. G. Myers Jr., Calcitonin receptor neurons in the mouse nucleus tractus solitarius control energy balance via the non-aversive suppression of feeding. *Cell Metab.* **31**, 301–312.e5 (2020).
36. J. A. Hardaway, L. R. Halladay, C. M. Mazzone, D. Pati, D. W. Bloodgood, M. Kim, J. Jensen, J. F. Di Berto, K. M. Boyt, A. Shiddapur, A. Erfani, O. J. Hon, S. Neira, C. M. Stanhope, J. A. Sugam, M. P. Saddoris, G. Tipton, Z. M. Elligott, T. C. Jhou, G. D. Stuber, M. R. Bruchas, C. M. Bulik, A. Holmes, T. L. Kash, Central amygdala prepronociceptin-expressing neurons mediate palatable food consumption and reward. *Neuron* **102**, 1037–1052.e7 (2019).
37. L. Toll, M. R. Bruchas, G. Calo', B. M. Cox, N. T. Zaveri, M. J. Christie, Nociceptin/orphanin FQ receptor structure, signaling, ligands, functions, and interactions with opioid systems. *Pharmacol. Rev.* **68**, 419–457 (2016).
38. J. Rodriguez-Romaguera, R. L. Ung, H. Nomura, J. M. Otis, M. L. Basiri, V. M. K. Namboodiri, X. Zhu, J. E. Robinson, H. E. van den Munkhof, J. A. McHenry, L. E. H. Eckman, O. Kosyk, T. C. Jhou, T. L. Kash, M. R. Bruchas, G. D. Stuber, Prepronociceptin-expressing neurons in the extended amygdala encode and promote rapid arousal responses to motivationally salient stimuli. *Cell Rep.* **33**, 108362 (2020).
39. L. A. Gunaydin, L. Grosenick, J. C. Finkelstein, I. V. Kauvar, L. E. Fenno, A. Adhikari, S. Lammel, J. J. Mirzabekov, R. D. Airan, K. A. Zalocusky, K. M. Tye, P. Anikeeva, R. C. Malenka, K. Deisseroth, Natural neural projection dynamics underlying social behavior. *Cell* **157**, 1535–1551 (2014).
40. T. A. Pologruto, R. Yasuda, K. Svoboda, Monitoring neural activity and [Ca^{2+}] with genetically encoded Ca^{2+} indicators. *J. Neurosci.* **24**, 9572–9579 (2004).
41. T. Yahiro, N. Kataoka, Y. Nakamura, K. Nakamura, The lateral parabrachial nucleus, but not the thalamus, mediates thermosensory pathways for behavioural thermoregulation. *Sci. Rep.* **7**, 5031 (2017).
42. B. N. Armbruster, X. Li, M. H. Pausch, S. Herlitze, B. L. Roth, Evolving the lock to fit the key to create a family of G protein-coupled receptors potently activated by an inert ligand. *Proc. Natl. Acad. Sci. U.S.A.* **104**, 5163–5168 (2007).
43. J. G. McCall, R. Al-Hasani, E. R. Siuda, D. Y. Hong, A. J. Norris, C. P. Ford, M. R. Bruchas, CRH engagement of the locus coeruleus noradrenergic system mediates stress-induced anxiety. *Neuron* **87**, 605–620 (2015).
44. R. Al-Hasani, J. G. McCall, G. Shin, A. M. Gomez, G. P. Schmitz, J. M. Bernardi, C.-O. Pyo, S. I. Park, C. M. Marcinkiewcz, N. A. Crowley, M. J. Krashes, B. B. Lowell, T. L. Kash, J. A. Rogers, M. R. Bruchas, Distinct subpopulations of nucleus accumbens dynorphin neurons drive aversion and reward. *Neuron* **87**, 1063–1077 (2015).
45. D.-o. Seo, S. C. Funderburk, D. L. Bhatti, L. E. Motard, D. Newbold, K. S. Girven, J. G. McCall, M. Krashes, D. R. Sparta, M. R. Bruchas, A GABAergic projection from the centromedial nuclei of the amygdala to ventromedial prefrontal cortex modulates reward behavior. *J. Neurosci.* **36**, 10831–10842 (2016).
46. P. Namburi, R. Al-Hasani, G. G. Calhoon, M. R. Bruchas, K. M. Tye, Architectural representation of valence in the limbic system. *Neuropsychopharmacology* **41**, 1697–1715 (2016).
47. J. C. Geerling, M. Kim, C. E. Mahoney, S. B. G. Abbott, L. J. Agostinelli, A. S. Garfield, M. J. Krashes, B. B. Lowell, T. E. Scammell, Genetic identity of thermosensory relay neurons in the lateral parabrachial nucleus. *Am. J. Physiol. Regul. Integr. Comp. Physiol.* **310**, R41–R54 (2015).
48. R. L. Miller, M. K. Stein, A. D. Loewy, Serotonergic inputs to FoxP2 neurons of the pre-locus coeruleus and parabrachial nuclei that project to the ventral tegmental area. *Neuroscience* **193**, 229–240 (2011).
49. R. Cintron-Colon, C. W. Johnson, J. R. Montenegro-Burke, C. Guijas, L. Faulhaber, M. Sanchez-Alavez, C. A. Aguirre, K. Shankar, M. Singh, A. Galmozzi, G. Siuzdak, E. Saez, B. Conti, Activation of kappa opioid receptor regulates the hypothermic response to calorie restriction and limits body weight loss. *Curr. Biol.* **29**, 4291–4299.e4 (2019).
50. L. Petreanu, D. Huber, A. Sobczyk, K. Svoboda, Channelrhodopsin-2–assisted circuit mapping of long-range callosal projections. *Nat. Neurosci.* **10**, 663–668 (2007).
51. K. T. Beier, E. E. Steinberg, K. E. De Loach, S. Xie, K. Miyamichi, L. Schwarz, X. J. Gao, E. J. Kremer, R. C. Malenka, L. Luo, Circuit architecture of VTA dopamine neurons revealed by systematic input-output mapping. *Cell* **162**, 622–634 (2015).
52. L. A. Schwarz, K. Miyamichi, X. J. Gao, K. T. Beier, B. Weissbourd, K. E. De Loach, J. Ren, S. Ibanes, R. C. Malenka, E. J. Kremer, L. Luo, Viral-genetic tracing of the input–output organization of a central noradrenaline circuit. *Nature* **524**, 88–92 (2015).
53. I. R. Wickersham, D. C. Lyon, R. J. O. Barnard, T. Mori, S. Finke, K.-K. Conzelmann, J. A. T. Young, E. M. Callaway, Monosynaptic restriction of transsynaptic tracing from single, genetically targeted neurons. *Neuron* **53**, 639–647 (2007).
54. M. A. Lebow, A. Chen, Overshadowed by the amygdala: The bed nucleus of the stria terminalis emerges as key to psychiatric disorders. *Mol. Psychiatry* **21**, 450–463 (2016).
55. T.-W. Chen, T. J. Wardill, Y. Sun, S. R. Pulver, S. L. Renninger, A. Baohan, E. R. Schreiter, R. A. Kerr, M. B. Orger, V. Jayaraman, L. L. Looger, K. Svoboda, D. S. Kim, Ultrasensitive fluorescent proteins for imaging neuronal activity. *Nature* **499**, 295–300 (2013).
56. J. A. Hardaway, N. A. Crowley, C. M. Bulik, T. L. Kash, Integrated circuits and molecular components for stress and feeding: Implications for eating disorders. *Genes Brain Behav.* **14**, 85–97 (2015).
57. O. Fu, Y. Iwai, K. Kondoh, T. Misaka, Y. Minokoshi, K.-i. Nakajima, SatB2-expressing neurons in the parabrachial nucleus encode sweet taste. *Cell Rep.* **27**, 1650–1656.e4 (2019).
58. S. Park, K. W. Williams, C. Liu, J.-W. Sohn, A neural basis for tonic suppression of sodium appetite. *Nat. Neurosci.* **23**, 423–432 (2020).
59. R. D. Palmiter, The parabrachial nucleus: CGRP neurons function as a general alarm. *Trends Neurosci.* **41**, 280–293 (2018).
60. D. L. Bhatti, A. T. Luskin, C. E. Pedersen, B. Mulvey, H. Oden-Brunson, K. Kimbell, A. Sawyer, R. W. Gereau IV, J. D. Dougherty, M. R. Bruchas, Extended amygdala-parabrachial circuits alter threat perception and encode homeostatic and hedonic feeding. bioRxiv 2020.03.03.975193 [**Preprint**]. 5 March 2020. https://doi.org/10.1101/2020.03.03.975193.
61. M. C. Chiang, E. K. Nguyen, M. Canto-Bustos, A. E. Papale, A.-M. M. Oswald, S. E. Ross, Divergent neural pathways emanating from the lateral parabrachial nucleus mediate distinct components of the pain response. *Neuron* **106**, 927–939.e5 (2020).
62. S. Choi, J. Hachisuka, M. A. Brett, A. R. Magee, Y. Omori, N.-u.-A. Iqbal, D. Zhang, M. M. De Lisle, R. L. Wolfson, L. Bai, C. Santiago, S. Gong, M. Goulding, N. Heintz, H. R. Koerber, S. E. Ross, D. D. Ginty, Parallel ascending spinal pathways for affective touch and pain. *Nature* **587**, 258–263 (2020).
63. L. Vong, C. Ye, Z. Yang, B. Choi, S. Chua Jr., B. B. Lowell, Leptin action on GABAergic neurons prevents obesity and reduces inhibitory tone to POMC neurons. *Neuron* **71**, 142–154 (2011).
64. M. J. Krashes, B. P. Shah, J. C. Madara, D. P. Olson, D. E. Strochlic, A. S. Garfield, L. Vong, H. Pei, M. Watabe-Uchida, N. Uchida, S. D. Liberles, B. B. Lowell, An excitatory paraventricular nucleus to AgRP neuron circuit that drives hunger. *Nature* **507**, 238–242 (2014).
65. J. G. McCall, E. R. Siuda, D. L. Bhatti, L. A. Lawson, Z. A. McElligott, G. D. Stuber, M. R. Bruchas, Locus coeruleus to basolateral amygdala noradrenergic projections promote anxiety-like behavior. *eLife* **6**, e18247 (2017).
66. J. T. Ting, T. L. Daigle, Q. Chen, G. Feng, in *Patch-Clamp Methods and Protocols*, M. Martina, S. Taverna, Eds. (Methods in Molecular Biology, Springer, 2014), pp. 221–242.
67. M. A. Rieger, D. M. King, B. A. Cohen, J. D. Dougherty, CLIP-seq and massively parallel functional analysis of the CELF6 RNA binding protein reveals a role in destabilizing synaptic gene mRNAs through interaction with 3'UTR elements in vivo. bioRxiv 401604 [**Preprint**]. 27 August 2018. https://doi.org/10.1101/401604.
68. A. M. Bolger, M. Lohse, B. Usadel, Trimmomatic: A flexible trimmer for Illumina sequence data. *Bioinformatics* **30**, 2114–2120 (2014).
69. B. Langmead, C. Trapnell, M. Pop, S. L. Salzberg, Ultrafast and memory-efficient alignment of short DNA sequences to the human genome. *Genome Biol.* **10**, R25 (2009).
70. A. Dobin, C. A. Davis, F. Schlesinger, J. Drenkow, C. Zaleski, S. Jha, P. Batut, M. Chaisson, T. R. Gingeras, STAR: Ultrafast universal RNA-seq aligner. *Bioinformatics* **29**, 15–21 (2013).
71. M. D. Robinson, D. J. McCarthy, G. K. Smyth, edgeR: A bioconductor package for differential expression analysis of digital gene expression data. *Bioinformatics* **26**, 139–140 (2010).
72. D. J. McCarthy, Y. Chen, G. K. Smyth, Differential expression analysis of multifactor RNA-Seq experiments with respect to biological variation. *Nucleic Acids Res.* **40**, 4288–4297 (2012).
73. M. K. Roth, B. Bingham, A. Shah, A. Joshi, A. Frazer, R. Strong, D. A. Morilak, Effects of chronic plus acute prolonged stress on measures of coping style, anxiety, and evoked HPA-axis reactivity. *Neuropharmacology* **63**, 1118–1126 (2012).

74. J. N. Betley, S. Xu, Z. F. H. Cao, R. Gong, C. J. Magnus, Y. Yu, S. M. Sternson, Neurons for hunger and thirst transmit a negative-valence teaching signal. *Nature* **521**, 180–185 (2015).
75. Y. Chen, Y.-C. Lin, T.-W. Kuo, Z. A. Knight, Sensory detection of food rapidly modulates arcuate feeding circuits. *Cell* **160**, 829–841 (2015).
76. A. G. Schindler, S. Li, C. Chavkin, Behavioral stress may increase the rewarding valence of cocaine-associated cues through a dynorphin/κ-opioid receptor-mediated mechanism without affecting associative learning or memory retrieval mechanisms. *Neuropsychopharmacology* **35**, 1932–1942 (2010).

Acknowledgments: We thank L. Lawson, D. Blumenthal, M. Chung, T. Hobbs, and C. Pizzano for animal colony maintenance; the Bruchas laboratory and UW NAPE Center for helpful discussions; J. G. McCall, B. A. Copits, and G. Stuber for assistance with electrophysiology. We thank R. Palmiter (HHMI, UW) for discussion and critiques regarding the manuscript. We thank C. Stander, K. Deisseroth, the Washington University HOPE Vector Core, and the UNC Vector Core for viral constructs, prep, and packaging. **Funding:** This study was supported by the National Institute on Mental Health (F31-MH122033 to A.T.L. and R01-MH112355 to M.R.B.), the National Institute on Drug Abuse (F31-DA051124 to C.E.P. and R01-DA033396 and P30-DA048736 to M.R.B.), the National Institute of Neurological Disorders and Stroke (R56-NS048602 and R01-NS106953 to R.W.G.), the National Institute of General Medical Sciences (T32-GM008151 to A.T.L.), and National Institute of Mental Health (F30-MH116654 to B.M. and U01-MH109133 to J.D.D.). Sequencing of TRAP samples was made possible in part by grant number UL1-RR024992 from the NIH–National Center for Research Resources. **Author contributions:** A.T.L., D.L.B., and M.R.B. conceptualized and designed the entire study. D.L.B and M.R.B. conceived the study. A.T.L., D.L.B., C.E.P., K.K., H.O.-B., T.B., and A.S. performed stereotaxic surgeries, behavioral experiments, and histology. D.L.B. and K.S.G. performed electrophysiological experiments. A.T.L. and C.E.P. performed fiber photometry experiments. A.T.L. and B.M. performed RNA-seq experiments. A.T.L., D.L.B., B.M., and C.E.P. performed the statistical analysis. A.T.L., D.L.B., and M.R.B. made the figures. A.T.L., D.L.B., and M.R.B. wrote the manuscript with collective input from all authors. J.D.D. supervised RNA-seq experiments. R.W.G. supervised electrophysiological experiments. M.R.B. supervised the entire study. **Competing interests:** Although there are no studies we report here that are related, for full disclosure, M.R.B. is a cofounder and scientific advisory board member for Neurolux Inc., a neurotechnology company. J.D.D. has previously received royalties related to the TRAP methodology. All other authors declare that they have no competing interests. **Data and materials availability:** All data needed to evaluate the conclusions in the paper are present in the paper and/or the Supplementary Materials. RNA-seq data are deposited in the NCBI GEO database with accession number GSE133484. Additional data related to this paper may be requested from the authors.

Submitted 16 June 2020
Accepted 14 January 2021
Published 26 February 2021
10.1126/sciadv.abd3666

Citation: A. T. Luskin, D. L. Bhatti, B. Mulvey, C. E. Pedersen, K. S. Girven, H. Oden-Brunson, K. Kimbell, T. Blackburn, A. Sawyer, R. W. Gereau IV, J. D. Dougherty, M. R. Bruchas, Extended amygdala-parabrachial circuits alter threat assessment and regulate feeding. *Sci. Adv.* **7**, eabd3666 (2021).

Extended amygdala-parabrachial circuits alter threat assessment and regulate feeding

Andrew T. Luskin, Dionnet L. Bhatti, Bernard Mulvey, Christian E. Pedersen, Kasey S. Girven, Hannah Oden-Brunson, Kate Kimbell, Taylor Blackburn, Abbie Sawyer, Robert W. Gereau IV, Joseph D. Dougherty and Michael R. Bruchas

Sci Adv **7** (9), eabd3666.
DOI: 10.1126/sciadv.abd3666